2021-08-19

Cardioprotective Role of Angiotensin-(1-7) In Heart Failure with Preserved Ejection Fraction

Edalat, Pariya

UNIVERSITY OF CALGARY

Cardioprotective Role of Angiotensin-(1-7) In Heart Failure with Preserved Ejection Fraction

by

Pariya Edalat

A THESIS

SUBMITTED TO THE FACULTY OF GRADUATE STUDIES

IN PARTIAL FULFILMENT OF THE REQUIREMENTS FOR THE

DEGREE OF MASTER OF SCIENCE

GRADUATE PROGRAM IN CARDIOVASCULAR AND RESPIRATORY SCIENCES

CALGARY, ALBERTA

AUGUST, 2021

Abstract

Heart failure with preserved ejection fraction (HFpEF) is a global health epidemic that accounts for half of the heart failure cases. Various therapeutic approaches have been tested to block the activation of the Renin-Angiotensin System (RAS), including AT1R blockers (ARBs), Angiotensin-converting enzyme (ACE) inhibitors (ACEi), and direct renin inhibitors (DRIs) with modest to negligible benefits. The Discovery of ACE2, a novel homolog of ACE, has advanced our understanding of the RAS. ACE2 is a monocarboxypeptidase that degrades Angiotensin II (Ang II) into Angiotensin-(1-7) (Ang-1-7), which works via the activation of the Mas receptor. It has been well understood that the actions of Ang-(1-7) attenuate cardiac remodeling, production of ROS, and cardiac fibrosis. Therefore, the objective of this study was to determine the therapeutic roles of Ang-(1-7) in HFpEF and identify the molecular mechanisms related to its actions. To generate a murine model of HFpEF, 10-12-weeks-old male mice were subjected to a high-fat diet (HFD) (including 60% Kcal fat) in addition to eNOS inhibition with L-NAME (0.5 g/L in drinking water). The Control group received a regular chow diet. The murine model of HFpEF was validated using the non-invasive transthoracic echocardiography and invasive pressure-volume (PV) loop analyses, which exhibited diastolic dysfunction as well as cardiac hypertrophy. To evaluate the effects of Ang-(1-7) on HFpEF, animals were administered with either saline or Ang-(1-7) (24 μg/kg/h) for four weeks. Ang-(1-7) treatment improved diastolic function by reducing isovolumetric relaxation time (IVRT), left ventricular end-diastolic pressure (LVEDP), and Tau value. The development of cardiac hypertrophy in the murine model of HFpEF was confirmed by wheat germ agglutinin (WGA) staining. Furthermore, by investigating different molecular pathways related to the development of hypertrophy, we indicated that the development of hypertrophy, fibrosis, and metabolic dysfunction in this study

was a result of partial activation of ERK1/2 and inactivation of AMPK, GSK3β, and PDH which did not significantly reverse with 4-weeks treatment of Ang-(1-7).

Preface

This thesis is an original, unpublished, independent work by the author Pariya Edalat. Echocardiography was performed by Dr. Darell Belke. PV loop was performed and analyzed by Dr. Vaibhav Patel. Tissue section preparation was performed by Dr. Xiong Chen at Libin's Institute Histopathology Core facilities. H&E and Masson Trichrome staining was performed under the supervision of Dr. Noura Ballasy. Tissue collection, glucose tolerance test, protein extraction and immunoblot analysis, WGA and PSR staining, imaging with Confocal microscope, and all the analyses for all the experiments in this study was done by the author Pariya Edalat.

Animal protocols used for the thesis were approved by the University of Calgary Animal Care Committee (AC17-0055).

Acknowledgements

First of all, I would like to express my gratitude to my supervisor, Dr. Vaibhav Patel, not only for giving me the opportunity for this amazing research experience but also for introducing me to the field of Cardiovascular sciences. Through his mentorship, I gained different laboratory techniques which gave me the ability to perform my experiments independently. Dr. Patel has given me the opportunity to present my data at several scientific sessions including The Basic Cardiovascular Sciences.

I would like to also thank my committee members, Drs. Jennifer Thompson and Robert Rose for their consistent support and guidance in the past two years. Their suggestions improved the quality of my research project.

I would like to give a special thanks to all the members of Patel's lab, Dr. Anshul Jadli, Dr. Karina Gomes, and particularly Dr. Noura Ballasy who gave me continuous support in the past two years. Noura welcomed me to the lab, taught me about cardiovascular physiology, and helped me to excel my skills in handling mice. She is not only an amazing fellow scientist but also a great friend.

From the bottom of my heart, I would like to thank my parents for their everyday support in all parts of my life. They made it possible for me to study abroad and experience an amazing life in Canada. They selflessly encouraged me to explore new directions in life and seek my destiny. This journey would not have been possible if not for them, and I dedicate this milestone to them.

Table of Contents

List of Illustrations and Figures

List of Abbreviations

Abbreviation	Definition
AMPK	AMP-Activated Protein Kinase
Ang I	Angiotensin I
Ang II	Angiotensin II
AT1R	Angiotensin II Type 1 Receptor
AT2R	Angiotensin II Type 2 Receptor
ARBs	Angiotensin Receptor Blockers
Ang-(1-7)	Angiotensin-(1-7)
Ang-(1-9)	Angiotensin-(1-9)
ACE	Angiotensin-Converting Enzyme
CCBs	Calcium Channel Blockers
CVDs	Cardiovascular Diseases
ACEi	Converting Enzyme Inhibitors
CAD	Coronary Artery Disease
cGMP	Cyclic Guanosine Monophosphate
Drp1	Dynamin-Related Protein 1
EF	Ejection Fraction
ET	Ejection Time
ESPVR	End Systolic Pressure Volume Relationship
EDPVR	End-Diastolic Pressure-Volume Relationship
eNOS	Endothelial Nitric Oxide Synthase

ECAR	Extracellular Acidification Rate
XF	Extracellular Flux
ERK1/2	Extracellular Signal-Regulated Kinases
FA	Fatty Acid
FS	Fractional Shortening
GLUT4	Glucose Transporter Type 4
GSK3β	Glycogen Synthase Kinase 3β
sGC	Guanylate Cyclase
H&E	Haematoxylin and Eosin
HF	Heart failure
HFmrEF	Heart Failure with mid-range Ejection Fraction
HFpEF	Heart Failure with preserved Ejection Fraction
HFrEF	Heart Failure with reduced Ejection Fraction
HFD	High-Fat Diet
SHR	Hypertensive Rat
HIF1α	Hypoxia-Inducible Factor 1α
IGF-1	Insulin-Like Growth Factor 1
IL	Interleukin
IVCT	Isovolumetric Contraction Time
IVRT	Isovolumetric Relaxation Time
JAK	Janus Kinases

LVH	Left Ventricular Hypertrophy
LV	Left Ventricular
LVDD	Left Ventricular Diastolic Dysfunction
LVEDD	Left Ventricular End-Diastolic Dimension
LVEDP	Left Ventricular End-Diastolic Pressure
LVESD	Left Ventricular End-Systolic Dimension
LVPWd	Left Ventricular Posterior Wall Thickness in Diastole
LVP	Left Ventricular Systolic Pressure
mTOR	Mammalian Target of Rapamycin
MasR	Mas Receptor
MAPK	Mitogen-Activated Protein Kinase
MCP1	Monocyte Chemoattractant Protein 1
MI	Myocardial Infarction
MIF	Myocardial Interstitial Fibrosis
NADPH	Nicotinamide Adenine Dinucleotide Phosphate
NO	Nitric Oxide
L-NAME	N-nitro-L-arginine methyl
OCR	Oxygen Consumption Rate
PBS	Phosphate-Buffered Saline
PIP3	Phosphatidylinositol (3,4,5)-trisphosphate
PI3K	Phosphoinositide 3-Kinase

PDK1	Phosphoinositide-Dependent Protein Kinase 1
PMA	Phosphomolybdic Acid
PSR	Picro Sirius Red
PGA	Polyglycolic Acid
PV	Pressure-Volume
PKA	Protein Kinase A
PKC	Protein Kinase C
PKG	Protein Kinase G
PDK4	Pyruvate Dehydrogenase Kinase 4
PDH	Pyruvate Dehydrogenase
ROS	Reactive Oxygen Species
RAS	Renin-Angiotensin System
RAAS	Renin-Angiotensin-Aldosterone-System
RT	Room Temperature
STAT	Signal Transducer and Activator of Transcription Proteins
TAGs	Triacylglycerol
TNFα	Tumour Necrosis Factor alpha
WGA	Wheat Germ Agglutinin
WAT	White Adipose Tissue
WHO	World Health Organization

Chapter 1: Introduction, Rationale, Hypothesis, and Aims

1.1. Epidemiology and clinical course of Heart Failure

According to World Health Organization (WHO), cardiovascular diseases (CVDs) are the leading cause of death globally, taking an estimated 17.9 million lives each year. Heart failure (HF), a major public health problem with an estimated prevalence of 27.7 million individuals worldwide, is a final common consequence of different CVDs, including sustained pressure overload, myocardial ischemia or infarction, volume overload, and inherited or acquired cardiomyopathies (Hilfiker-Kleiner, Landmesser et al. 2006, Ho, Gona et al. 2012). HF is defined as a syndrome and characterized by an impaired ability of the heart to fill with or eject blood equivalent to meet metabolic needs of the body, resulting in signs of pulmonary and systemic venous congestion (Sharma and Kass 2014).

Left ventricular (LV) ejection fraction (EF) is widely used to define the unique differences among individuals with the clinical syndrome of HF (Dunlay, Roger et al. 2017). Based on LVEF, HF patients are classified as presenting reduced EF (HFrEF; EF≤ 40%) or preserved EF (HFpEF) (Dunlay, Roger et al. 2017). Although the standard definition of HFpEF is different in various studies, the latest guidelines limit the designation of HFpEF to patients with EF≥ 50%, and those with EF of 41-49% are considered as mid-range EF (HFmrEF) (Dunlay, Roger et al. 2017). HFmrEF patients are deemed to have an intermediate characteristic between HFpEF and HFrEF: they are younger, more likely to be male, and less frequently have hypertension compared with those with HFpEF, while the mortality rate at one-year study lies between HFrEF and HFpEF patients (Chioncel, Lainscak et al. 2017). Besides LVEF, patients with HFpEF differ from HFrEF patients in several distinctive ways: HFpEF patients are older,

more often hypertensive, and less likely to have coronary artery disease (CAD). One of the most important differences between these two groups is the number of female patients, accounting for approximately 63% of all HFpEF patients, while females only account for 38% of all HFrEF patients (Borlaug and Redfield 2011). Furthermore, LV chamber dilation is a crucial characteristic of HFrEF. While the ventricular chamber size remains normal in patients with HFpEF, LV wall thickness, the ratio of wall thickness to chamber dimension, and the ratio of ventricular mass to chamber volume is often increased in patients with HFpEF compared to healthy controls as well as patients with HFrEF (Borlaug and Redfield 2011). Arterial loading conditions are different among HFpEF and HFrEF patients: although vasoconstriction is common to both forms of HF, the pulse pressure is higher in HFpEF which produces higher blood pressure lability with changes in preload, afterload, and hemodynamic stress in HFpEF (Borlaug and Redfield 2011). It is also important to note that although the prevalence of HFpEF and HFrEF is equal among HF cases and mortality rate increases similarly in both groups, there are clear differences in cause of death between the two subtypes of HF: cardiovascular causes of deaths is lower in HFpEF patients compared with HFrEF (Ho, Gona et al. 2012). Non-cardiovascular conditions that commonly contributed to death of patients with HFpEF were renal disease and diabetes (Lee, Gona et al. 2011).

1.2. Heart Failure with preserved Ejection Fraction

Approximately, half of the patients with signs and symptoms of HF, exhibit preserved EF. Alongside preserved EF, diastolic dysfunction is a critical characteristic of HFpEF, which is evidenced by elevated filling pressure, abnormal LV relaxation, and increased left ventricular chamber stiffness (Zile, Baicu et al. 2004). However, there is a notable difference between patients with diastolic dysfunction (LVDD) and patients with HFpEF, which can be attributed to

comorbidities observed in patients with HFpEF (Glezeva and Baugh 2014). Hypertension, an important risk factor for HF, is common in most patients with HFpEF. Diabetes accounts for 20-40% of patients with HFpEF, and patients with HFpEF are also more likely to be obese than patients with HFrEF (Owan, Hodge et al. 2006).

1.2.1. Clinical Trials for HFpEF

Major neutral trials for patients with HFpEF include the studies of β-blockers, angiotensin-converting enzyme inhibitors (ACEi), angiotensin receptor blockers (ARBs), aldosterone antagonists, and calcium channel blockers (Kanwar, Walter et al. 2016). The Renin-Angiotensin-Aldosterone-System (RAAS) and β-adrenergic stimulation pathways have been targeted due to their link to hypertension, fibrosis, and fluid imbalance, the latter to improve time for diastolic LV filling (Sharma and Kass 2014). Although many of these trials were successful in patients with HFrEF, no clinical trials, to date, have shown benefits in patients with HFpEF. Current standard therapies do not affect mortality in HFpEF. Moreover, only a few of the clinical trials have shown modest symptomatic improvement in patients with HFpEF (Sharma and Kass 2014).

The SENIORS Study (Study of the Effect of Nebivolol Intervention on Outcomes and Rehospitalisation in Seniors with Hearth Failure) investigated the effect of nebivolol, a β1-selective blocker with vasodilating properties related to nitric oxide modulation, on mortality and morbidity in elderly patients with HF regardless of ejection fraction (Flather, Shibata et al. 2005). Sub analysis of this trial compared patients with HFpEF (EF>35%) to the patients with HFrEF (EF≤35%). Although all-cause mortality or hospitalization for cardiovascular causes was not significantly different between the two groups, it is still not completely evident whether β-blockers have the same results in HFpEF as in HFrEF (Kanwar, Walter et al. 2016).

The PEP-CHF (Perindopril in Elderly People with Chronic Heart Failure) study, investigated the effects of ACE-inhibitors on morbidity and mortality in patients with the clinical diagnosis of diastolic heart failure (Cleland, Tendera et al. 2006). Perindopril, an ACE inhibitor, had no significant benefits compared with placebo on long-term morbidity and mortality in patients with diastolic HF. However, improved symptoms and exercise capacity, and HF-related hospitalization had been indicated, making it a potentially viable, albeit non-optimal, treatment option (Cleland, Tendera et al. 2006). The use of ARBs has also been studied in different clinical trials, including I-PRESERVE (Irbesartan in Heart Failure with Preserved Ejection Fraction). Similar to ACE inhibitors, irbesartan exhibited no significant benefit on cardiovascular outcomes, including mortality from any cause and hospitalization for cardiovascular cause, in patients with HFpEF (Massie, Carson et al. 2008). The ALDO-DHF (Effect of Spironolactone on Diastolic Function and Exercise Capacity in Patients with Heart Failure with Preserved Ejection Fraction) study evaluated the effect of an aldosterone antagonist in HFpEF with the primary end points being improved diastolic function and exercise capacity (Edelmann, Wachter et al. 2013). Although this study showed some improvements in diastolic function, maximal exercise capacity, clinical symptoms, and quality of life were unchanged (Edelmann, Wachter et al. 2013). Using calcium channel blockers (CCBs) such as verapamil, in older HFpEF patients was shown to improve exercise capacity, however, CCBs had no associations with individual endpoints of mortality or HF hospitalization (Hung, Cherng et al. 2002). In RELAX (The Effect of Phosphodiesterase 5 Inhibition on Exercise Capacity and Clinical Status in Heart Failure with Preserved Ejection Fraction) clinical trial, the effect of the phosphodiesterase-5 inhibitor, sildenafil, was compared with placebo on exercise capacity and clinical status in HFpEF (Redfield, Chen et al. 2013). Although previous studies on different HF animal models showed

beneficial effects of PDE5A, RELAX outcomes were neutral, reporting no benefit of sildenafil compared with placebo in the primary end point or any secondary functional and structural end points including exercise capacity or clinical status (Redfield, Chen et al. 2013).

Although many of these clinical trials had beneficial effects on HFrEF, none of these studies showed improvement in hospitalization or mortality rate in patients with HFpEF. Outcomes of these clinical trials strongly suggest the differential molecular mechanisms involved in the pathogenesis of HFrEF and HFpEF. Hence, currently available treatment for HFrEF may not be ideal in patients with HFpEF. Current deficiency in the clinical management of patients with HFpEF is largely due to inadequate understanding of the underlying mechanisms and knowledge of the key molecular players. Therefore, an in-depth understanding of molecular mechanisms involved in the pathogenesis of HFpEF is extremely warranted.

1.2.2. Molecular mechanisms of HFpEF

Although LV diastolic dysfunction is one of the key defining features of HFpEF (Ponikowski, Voors et al. 2016), different cellular and molecular mechanisms related to various comorbidities in HFpEF patients have an essential role in developing the syndrome. Comorbidities, including obesity and diabetes, induce the chronic proinflammatory state that contributes to increased myocardial production of Reactive Oxygen Species (ROS), including superoxide, hydrogen peroxide, and hydroxyl radical (Hilfiker-Kleiner, Landmesser et al. 2006, Paulus and Tschöpe 2013). Inflammation can also lead to pathological hypertrophy which is often associated with impaired myocardial vascularization, adverse remodeling of extracellular matrix composition, and fibrosis (De Boer, Pinto et al. 2003). Furthermore, insufficient activation of different cytokines and neurohormonal factors such as RAAS, catecholamines, and endothelin, along with increased free radicals and nitrotyrosine levels, limited bioavailability of

nitric oxide (NO), and impaired myocardial cyclic guanosine monophosphate (cGMP) and Protein Kinase G (PKG) signaling, have an essential role in early and late cardiac remodeling in LV diastolic dysfunction and HFpEF (Glezeva and Baugh 2014) (Figure 1).

1.2.2.1. Impaired inflammatory signaling

Different studies have indicated that patients with HF have higher levels of pro-inflammatory cytokines such as Tumour Necrosis Factor alpha (TNFα), interleukin (IL) 1, IL6, IL8, and monocyte chemoattractant protein 1 (MCP1) (Adamopoulos, Parissis et al. 2001, Mann 2002, Torre-Amione 2005) (Figure 1). It has been shown that comorbidities commonly present with HFpEF, including diabetes and obesity, can induce a systemic and chronic inflammatory state (Paulus and Tschöpe 2013). Early vascular inflammation is the most common precursor of comorbidities prevalent in HFpEF, such as hypertension, atherosclerosis, and CAD (Kalogeropoulos, Georgiopoulou et al. 2010). Furthermore, macrophage infiltration of adipose tissue in visceral obesity is a critical determinant of systemic inflammatory state due to the secretion of proinflammatory cytokines (Taube, Schlich et al. 2012). Additionally, salt-sensitive hypertension and high salt intake, both of which are known to be associated with HFpEF in rodent models, cause oxidative stress, conceivably due to renal production of proinflammatory cytokines (Tian, Moore et al. 2007). A recent study revealed that the systemic inflammatory state induced by these comorbidities could be predictive of HFpEF incidents but not of HFrEF incidents (Kalogeropoulos, Georgiopoulou et al. 2010). The systemic inflammatory state triggered by HFpEF comorbidities can influence the coronary microvascular endothelium (van Heerebeek, Hamdani et al. 2008, Westermann, Lindner et al. 2011). Proinflammatory cytokines and comorbidities such as diabetes and systemic inflammatory state can also cause the production of ROS through the activation of nicotinamide adenine dinucleotide phosphate

(NADPH) oxidase (Griendling, Sorescu et al. 2000, Shenouda, Widlansky et al. 2011). Increased production of ROS can cause endothelial dysfunction and subsequent decrease in vascular bioavailability of NO leading to impaired soluble guanylate cyclase (sGC) pathway and reduced cGMP levels (Schulz, Jansen et al. 2008, Paulus and Tschöpe 2013) (Figure 1).

1.2.2.2. cGMP-PKG signaling deficiency.

PKG activates myosin light chain phosphatase that reduces phosphorylation of myosin light chain, resulting in relaxation of vascular smooth muscle cells (Surks, Mochizuki et al. 1999). Depressed endothelial NO generation is a primary cause of reduced cGMP-PKG signaling in cardiomyocytes (Paulus and Tschöpe 2013). Stimulation of the NO-cGMP-PKG pathway generally leads to antihypertrophic, antifibrotic, and pro-angiogenic effects in the myocardium (Takimoto, Champion et al. 2005). Low PKG activity can increase cardiomyocyte hypertrophy and stiffness and delay cardiomyocyte relaxation (Brutsaert 2003, van Heerebeek, Hamdani et al. 2012). PKG also phosphorylates and enhances the proteasomal clearance of misfolded proteins and stimulates autophagy, playing a key role in anti-inflammatory effects, improvement of mitochondrial energetics, and reversal of the signaling effects of obesity (Mitschke, Hoffmann et al. 2013, Inserte and Garcia-Dorado 2015, Mishra and Kass 2021). PKG along with protein kinase A (PKA), can make the giant cytoskeletal protein, titin, more compliant (Krüger, Kötter et al. 2009). Titin acts as a bidirectional spring and has an essential role in the early diastolic recoil and late diastolic distensibility of cardiomyocytes (Paulus and Tschöpe 2013). Reduced PKG activity and lower cGMP concentration was indicated in concentrically remodeled LV myocardium of patients with HFpEF (van Heerebeek, Hamdani et al. 2012).

1.2.2.3. Cardiac hypertrophy

Although left ventricular hypertrophy (LVH) is only present in 30-60% of patients with HFpEF, LVH is one of the most-studied aspects of HFpEF and has long been considered to be a key mediator of HFpEF, and an essential cause of diastolic dysfunction and elevated diastolic filling pressures (Zile, Gottdiener et al. 2011, Reddy, Carter et al. 2018, Mishra and Kass 2021). Pathological hypertrophy is usually accompanied by interstitial and perivascular fibrosis and cardiomyocyte death, along with elevated levels of type I collagen and myofibroblast activation (Nakamura and Sadoshima 2018). Pathological hypertrophy is also a result of impaired Ca^{2+} handling, myocardial fibrosis, oxidative stress, cell death, insufficient angiogenesis, mitochondrial dysfunction, metabolic reprogramming, abnormal cell growth and protein synthesis, and induction of fetal gene programming; the features that can also occur in HFpEF (Nakamura and Sadoshima 2018, Mohammed, Hussain et al. 2015, Dunlay, Roger et al. 2017). G protein-coupled receptors such as β-adrenergic receptors, stress hormone ligands including angiotensin II (Ang II), and signaling kinases such as AMPK, ERK1/2, mTOR, and p38-MAPK are among the key molecular contributors to the development of pathological hypertrophy (Mishra and Kass 2021). The Phosphoinositide 3-kinase (PI3K) catalytic subunit p110α is essential for physiological, but not pathological hypertrophy, where activation of PI3Kp110α in the heart can promote physiological hypertrophy and antagonize pathological hypertrophy (McMullen, Shioi et al. 2003). AKT is an important downstream serine/threonine-protein kinase, activated by Phosphatidylinositol (3,4,5)-trisphosphate (PIP3)-mediated membrane recruitment and phosphoinositide-dependent protein kinase 1 (PDK1) (Weeks, Gao et al. 2012). It has been indicated that inhibition of AKT can lead to maladaptive hypertrophy (Haq, Choukroun et al. 2000). Furthermore, phosphorylation and inhibition of glycogen synthase kinase 3β (GSK3β) by

insulin and insulin-like growth factor 1 (IGF-1), through PI3K/AKT pathways, develop compensated cardiac hypertrophy (Wang, Wang et al. 2000, Hirotani, Zhai et al. 2007, Markou, Cullingford et al. 2008). Another key target of AKT is the mammalian target of rapamycin (mTOR), a serine/threonine-protein kinase primarily known for its role in protein synthesis. mTOR functions as part of two distinct complexes, mTORC1 and mTORC2, to correlate with growth factor signaling and nutrient availability with cell metabolism and growth by regulating protein synthesis and degradation (Saxton and Sabatini 2017). mTOR activity can be increased both in physiological and pathophysiological hypertrophy in response to biomedical, mechanical, and metabolic signals (Nakamura and Sadoshima 2018). Furthermore, AMP-activated protein kinase (AMPK) inhibits mTORC1, and pharmacological suppression of mTORC1 with rapamycin, a specific inhibitor of mTOR, decreases angiotensin II-induced and pressure-overload-induced pathological hypertrophy and heart failure (Shioi, McMullen et al. 2003). Endothelial nitric oxide synthase (eNOS), another important downstream signaling molecule of AKT, is a primary source of NO production, which is a modulator of exercise-induced cardiac hypertrophy. It has been indicated that exercise-mediated stimulation of eNOS and NO attenuates pathological hypertrophy through activation of β_3-adrenergic receptors and PKG (Calvert, Condit et al. 2011).

1.2.2.4. Mitochondrial and metabolic defects

Alterations in systemic and cardiac metabolism have been correlated with the development of heart failure. Impaired adaptation of energy metabolism during hypertrophic response worsens pathological hypertrophy and increases cardiomyocyte death (Liew, Xu et al. 2017, Nakamura and Sadoshima 2018). The development of cardiac dysfunction is usually accompanied by a reduction in rates of fatty acid (FA) oxidation (Doenst, Nguyen et al. 2013).

The decline in FA oxidation may be secondary to inhibition of Peroxisome Proliferator-Activated Receptor α (PPARα) signaling and activation of the hypoxia-inducible factor 1α (HIF1α)-PPARγ signaling axis, which impairs FA transport into mitochondria and downregulates FA oxidative enzymes (Sack, Rader et al. 1996). It is important to note that although there is a decline in cardiac FA oxidation rates, plasma levels of FA are increased in the late stages of HF (Bertero and Maack 2018). The mismatch between FA uptake and oxidation causes intracellular accumulation of lipids, which are partly stored as Triacylglycerol (TAGs) but can also be channeled into non-oxidative pathways, generating toxic lipid species, such as ceramide and diacylglycerol. Such lipotoxicity results in mitochondrial dysfunction and apoptosis and has a role in the progression of HF (Goldberg, Trent et al. 2012). Furthermore, the failing heart is considered to have increased glucose uptake and rate of glycolysis, while the rate of glucose oxidation remains unchanged (Bertero and Maack 2018). Impaired glucose oxidation, as a result of defective mitochondrial oxidative metabolism and myocardial insulin resistance, leads to pressure overload, while FA utilization is only moderately affected or has no influence on this setting (Zhabyeyev, Gandhi et al. 2013, Fukushima and Lopaschuk 2016). As evident from these studies, metabolic dysfunction in the hearts with HFrEF are validated and has provided some of the very important targets with therapeutic potential, including Pyruvate Dehydrogenase Kinase 4 (PDK4) and Pyruvate dehydrogenase (PDH). Due to the lack of an ideal mouse model of HFpEF, metabolic perturbations in hearts with HFpEF remain to be studied.

1.3. The potential cardioprotective role of Angiotensin-(1-7) in HFpEF

1.3.1. Renin-angiotensin system

The renin-angiotensin system (RAS) is one of the most potent regulators of cardiovascular (patho)physiology, and an important target for therapeutics (Santos, Oudit et al. 2019). RAS is a complex network mediating cardiovascular and renal homeostasis. Ang II, an active metabolite and a key mediator of RAS activity is produced by sequential enzymatic cleavage of angiotensinogen, which is primarily produced in the liver (Parajuli, Ramprasath et al. 2014). In the bloodstream, the circulating angiotensinogen is converted by renin to a decapeptide, Angiotensin I (Ang I), which is further converted to an octapeptide, Ang II, by Angiotensin-Converting Enzyme (ACE). Ang II applies its biological effects by binding to either the angiotensin II type 1 receptor (AT1R) or the angiotensin II type 2 receptor (AT2R) (Volpe, Musumeci et al. 2003, Gomes, Santos et al. 2012). Physiologically, AT1R activation by Ang II evokes vasoconstriction, water intake, and Na^+ retention, while activation of AT2R antagonizes the effects of AT1R preventing its hypertrophic and angiogenic effects (Steckelings, Widdop et al. 2010, Gomes, Santos et al. 2012, Santos, Oudit et al. 2019). However, RAS imbalance to a state of predominant ACE/Ang II/AT1R axis signaling is also known to be involved in the underlying pathogenic mechanisms of hypertension, oxidative stress, cardiac hypertrophy, myocardial fibrosis, and inflammation, leading to onset and progression of cardiovascular diseases (Keidar, Kaplan et al. 2007). Various clinical trials have tested ACEi or ARBs on patients with HFrEF as well as HFpEF. Although many of these clinical trials showed improved outcomes in patients with HFrEF, ACEi and ARBs remain ineffective on patients with HFpEF, where the rate of hospitalization and mortality remained unaffected (Cleland, Tendera et al. 2006, Massie, Carson et al. 2008, Kanwar, Walter et al. 2016, Ponikowski, Voors et al. 2016).

ACE2, a homolog of ACE, is a monocarboxypeptidase that degrade Ang I to a nonapeptide, Angiotensin-(1-9) (Ang-(1-9)), and Ang II to a heptapeptide, Angiotensin-(1-7) (Ang-(1-7)). Ang-(1-7) acts via activation of Mas receptor (MasR) and counteracts the classical arm of RAS (ACE/Ang II/AT1R) leading to vasodilatory, anti-inflammatory, antifibrotic, and anti-apoptotic effects, exhibiting beneficial effects in the setting of cardiovascular disease. ACE2 is robustly expressed in different organ systems, including the cardiovascular system, kidneys, lungs, and brain, in which it performs an essential role in maintaining cardiovascular homeostasis (Gembardt, Sterner-Kock et al. 2005, Keidar, Kaplan et al. 2007).

1.3.2. Angiotensin-(1-7)

In the heart, ACE2 is localized in cardiomyocytes, cardiac fibroblasts, and coronary vascular endothelium (Patel, Zhong et al. 2014). The major source of Ang-(1-7) in murine and human hearts is via proteolytic cleavage of Ang II by ACE2. However, plasma Ang-(1-7) is primarily generated by neprilysin from Ang I, and blocking neprilysin leads to lower plasma Ang-(1-7) levels and greater Ang II levels (Pavo, Wurm et al. 2016). MasR, a primary receptor of Ang-(1-7) is also present on cardiomyocytes, cardiac fibroblasts, and endothelial cells (Sampaio, Souza dos Santos et al. 2007). Activation of MasR by Ang-(1-7) results in various effects that antagonize the effects of Ang II/AT1R activation (Mercure, Yogi et al. 2008), hence Ang-(1-7) and Ang II are deemed as “physiological antagonists”. MasR activation triggers the activation of PI3K-AKT-eNOS and inhibition of protein kinase C-p38 mitogen-activated protein kinase (PKC-p38 MAPK) pathways, leading to reduced collagen expression and cardiac fibrosis (Figure 2) (Sampaio, Souza dos Santos et al. 2007). Furthermore, exogenous administration of Ang-(1-7) inhibited the production of cardiac fibrosis in models of pressure overload induced by DOCA-salt hypertension, chronic Ang II treatment, L-NAME hypertension, and diabetic

cardiomyopathy (Benter, Yousif et al. 2006, Grobe, Mecca et al. 2006, Grobe, Mecca et al. 2007, Hao, Yang et al. 2015). Activation of MasR by Ang-(1-7) in neonatal cardiomyocytes has also been shown to inhibit MAPK extracellular signal-regulated kinases (ERK1/2) activity, preventing the cell growth and hypertrophy (Tallant, Ferrario et al. 2005). Moreover, Ang-(1-7) mediates the activity of GSK3β by preventing its inactivation by Ang II, the activity that supports the anti-hypertrophic effect of Ang-(1-7) in the heart and in cardiomyocytes (Tallant, Ferrario et al. 2005, Gomes, Lara et al. 2010) (Figure 2). Increased activity of ACE2/Ang-(1-7)/MasR axis decreases the pro-inflammatory cytokines such as TNF-α, IFN-γ, IL-1β, and IL-6, while enhancing the anti-inflammatory cytokine, IL-10 (Sukumaran, Veeraveedu et al. 2011, Sukumaran, Veeraveedu et al. 2012, Patel, Mori et al. 2016). A large body of evidence has indicated increased levels of proinflammatory cytokines in HFpEF, leading to increased level of ROS, development of cardiac remodeling, reduced level of NO bioavailability, and decreased level of cGMP (De Boer, Pinto et al. 2003, Hilfiker-Kleiner, Landmesser et al. 2006, Paulus and Tschöpe 2013, Glezeva and Baugh 2014). Therefore, anti-fibrotic, anti-inflammatory, and anti-hypertrophic effects of Ang-(1-7) can be beneficial for HFpEF therapeutics. Importantly, although ACE2/Ang-(1-7)/MasR axis has shown a clear negative regulation of ACE/Ang II/AT1R axis, exhibiting potent cardio- and vascular-protective roles in preclinical models (Iusuf, Henning et al. 2008, Santos, Ferreira et al. 2013), a clinical trial looking at cardioprotective effects of Ang-(1-7) or ACE2 on patients with HFpEF remains to be conducted.

1.4. Rationale and Hypothesis

Cardioprotective roles of Ang-(1-7) has been established by extensive preclinical investigations on a number of cardiovascular diseases: transgenic animals with an 8-fold increase in Ang-(1-7) peptide had significantly less ventricular hypertrophy and fibrosis than their non-

transgenic littermates in response to a hypertensive challenge (Mercure, Yogi et al. 2008); Ang-(1-7) treatment improved glucose intolerance, epicardial adipose tissue inflammation, and cardiac insulin resistance (Patel, Mori et al. 2016); contribution of Ang-(1-7) to the beneficial effects of AT1R blockers on cardiac dysfunction and ventricular remodeling after myocardial infarction had also been indicated (Tallant, Ferrario et al. 2005). Most importantly, the key role of Ang-(1-7) in protecting against cardiovascular disease has been demonstrated by Patel et al., (2015), in a study using blockade of Ang-(1-7) receptor was shown to suppress therapeutic roles of ACE2 (Patel, Takawale et al. 2015). Furthermore, considering the fact that Ang-(1-7) has direct and indirect effects on many of the pathways involved in cardiac hypertrophy and impaired cardiac metabolism, we hypothesised that administration of Ang-(1-7) will slow down the development of cardiac hypertrophy, diastolic dysfunction, and metabolic changes in HFD+L-NAME-induced HFpEF in a murine model.

1.5. Specific Aims

To address this hypothesis, my research project investigated the following aims:

1. Investigate the effects of Ang-(1-7) on comorbidities associated with HFpEF in a murine model.
2. Determine the effects of Ang-(1-7) on HFpEF-associated cardiac remodeling and diastolic dysfunction.
3. Evaluate the effects of Ang-(1-7) on various molecular pathways related to cardiac hypertrophy and metabolic dysfunction.

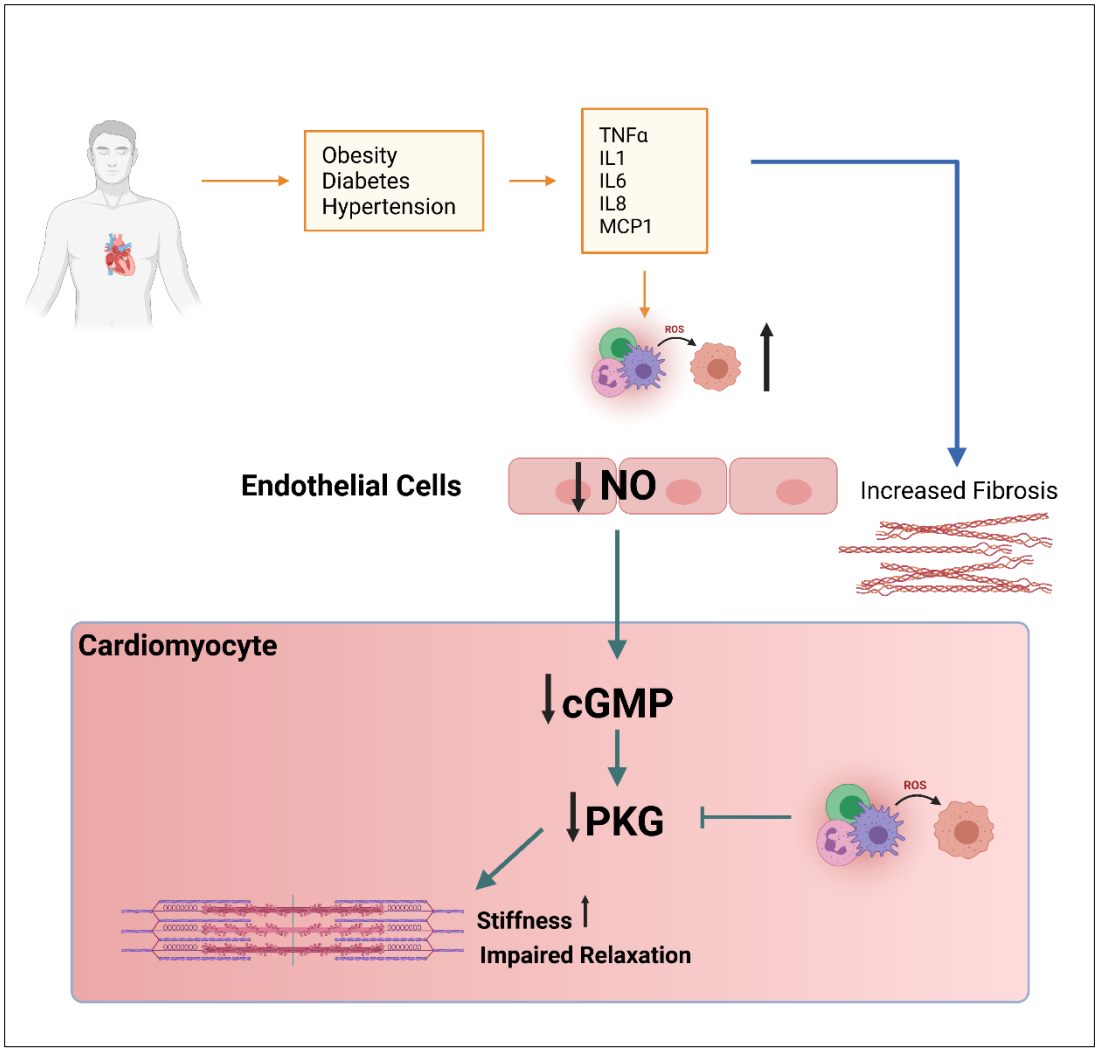

Figure 1. The summary of molecular mechanisms involved in the development of HFpEF. Different comorbidities such as obesity, diabetes, and hypertension lead to increased levels of proinflammatory cytokines which results in an ROS production. Increased levels of ROS leads to reduced bioavailability of NO, decreased level of cGMP, and reduced activity of PKG. The lower level of PKG activity results in cardiomyocyte remodeling by increasing stiffness and impaired relaxation. Proinflammatory cytokines also increase the level of fibrosis which leads to cardiac remodeling (Created with BioRender.com).

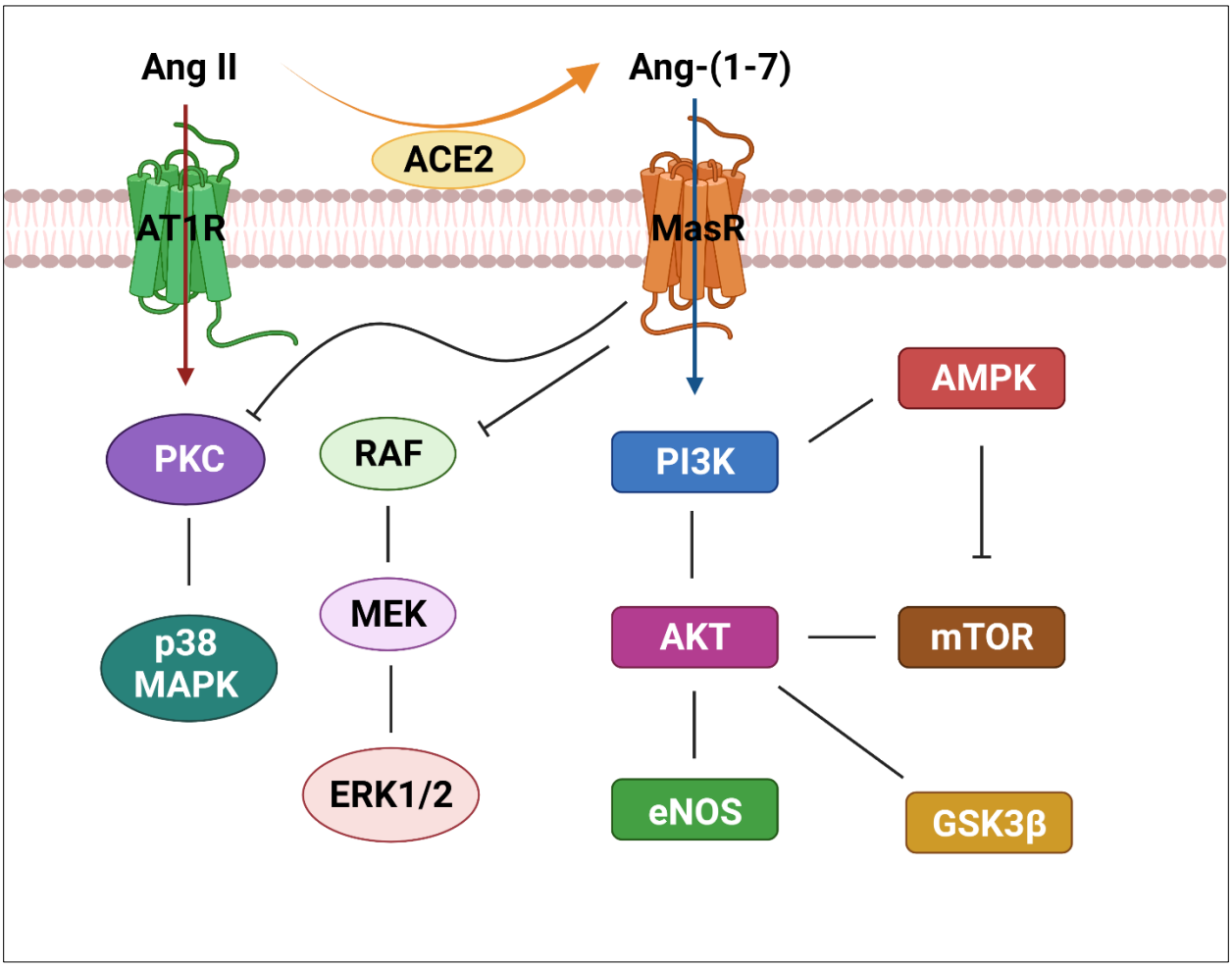

Figure 2. ACE2/Ang-(1-7)/MasR action through different molecular pathways. Activation of MasR by Ang-(1-7) triggers the activation of PI3K/AKT/eNOS and inhibition of PKC/p38 MAPK pathways, leading to reduced collagen expression and cardiac fibrosis. The activation of MasR by Ang-(1-7) also inhibits MAPK ERK1/2 activity, mediates GSK3β, and activates PKG by increasing NO bioavailability (Created with BioRender.com).

Chapter 2: Animal model, Materials, and Methodology

2.1. Murine model of HFpEF

The use of murine models is a valuable tool in understanding the pathophysiology of various CVDs. Indeed, the lack of adequate understanding of the underlying mechanism of HFpEF can be largely attributed to the lack of an ideal murine model. HFpEF is a complex syndrome in which individual patients who develop the disease are different in the comorbidities they demonstrate (Valero-Muñoz, Backman et al. 2017). An ideal animal model must meet diverse requirements to mimic human disease, including cardiac, hemodynamic, neurohormonal, and peripheral aberrations commonly observed in HFpEF patients (Halapas, Papalois et al. 2008). The most common murine models include hypertension-induced HFpEF as well as models of HFpEF associated with the metabolic phenotype (Valero-Muñoz, Backman et al. 2017). Some of the most studied hypertensive HFpEF murine models include Dahl-salt sensitive rats, DOCA salt-induced hypertension, Ang II-infusion in mice, spontaneously hypertensive rat (SHR), and thoracic aortic constriction-induced pressure overload in mice (Valero-Muñoz, Backman et al. 2017). Although these models replicate many of the clinical features observed in patients with HFpEF, a major drawback with these models is their transition from HFpEF to HFrEF, which is very uncommon in patients with HFpEF (Valero-Muñoz, Backman et al. 2017).

Two of the most widely used murine models with metabolic phenotypes are db/db and ob/ob mice, which harbors mutations in genes encoding leptin receptor and leptin, respectively. Due to the disruption in the leptin-mediated satiety, both these mutant mice eat excessively and represent obesity, hyperglycemia, and diastolic dysfunction (Barouch, Berkowitz et al. 2003, Christoffersen, Bollano et al. 2003, Lindström 2007, Reil, Hohl et al. 2013). Although murine

models of obesity and diabetes-induced diastolic dysfunction represent many of the comorbidities associated with HFpEF, they also exhibit various key differences compared to a clinical HFpEF phenotype. For example, uncontrolled severe hyperglycemia and insulin resistance observed in murine db/db and ob/ob models do not mimic the metabolic disorders of clinical HFpEF phenotype (Konduracka, Gackowski et al. 2007). Furthermore, in the absence of obesity, on the onset of HFpEF, there is limited information regarding an obesity model alone that does not have insulin resistance or diabetes, which therefore restricts studying the exclusive role of enhanced adiposity in HFpEF (Valero-Muñoz, Backman et al. 2017).

Recently, a novel murine model of HFpEF was developed using two of the most common co-morbidities observed in patients with HFpEF, known as a "two-hit mouse model of HFpEF." Schiattarella et al. exposed 8-10-week-old male C57BL/6 wild-type (WT) mice to a high-fat diet (HFD), containing 60% of kilocalories from fat, and N-nitro-L-arginine methyl (L-NAME**;** 0.5 g/L in drinking water), which featured different comorbidities common in clinical HFpEF phenotype (Schiattarella, Altamirano et al. 2019). HFD-induced an increase in body weight and glucose intolerance, whereas L-NAME treatment raised systolic and diastolic blood pressure (Schiattarella, Altamirano et al. 2019). These animals displayed preserved LVEF for 15 weeks as well as varying degrees of diastolic dysfunction and pulmonary congestion, making it a valuable HFpEF murine model (Schiattarella, Altamirano et al. 2019). The major shortcoming of the existing rodent model of HFpEF, eventual transition to HFrEF, was overcome by the murine model developed by Schiattarella et al. (Lim 2019, Schiattarella, Altamirano et al. 2019). Considering the recapitulation of various clinical features and comorbidities of HFpEF (diastolic dysfunction, pulmonary congestion, obesity, hypertension, and exercise intolerance), the two-hit mouse model of HFpEF proves to be highly suitable for our experimental investigations. Hence,

in this study, we employed the same mouse model to investigate the cardioprotective roles of Ang-(1-7) in HFpEF.

2.2. Experimental Animals

All experiments were performed following the University of Calgary institutional guidelines, which are in line with the Canadian Council on Animal Care and the Guide for the Care and Use of Laboratory Animals published by the U.S. National Institutes of Health.

Male C57BL/6J wild-type mice, aged 10-12 weeks, were fed with a HFD (containing 60% kilocalories from fat) along with L-NAME (0.5 g/L) in their drinking water for 15 weeks to generate a murine model of HFpEF, as previously described (Schiattarella, Altamirano et al. 2019). Control mice received a regular chow diet. All the mice were given water *ad libitum* (Figure 3).

2.3. Osmotic pump implantation

To determine the potential cardioprotective effects of Ang-(1-7), after 11 weeks of HFD+L-NAME, mice were randomly divided into two groups: The first group received Alzet osmotic pumps filled with Ang-(1-7) (release rate of 24 µg/Kg/h), whereas the second group received saline (as a vehicle) perfusion and served as HFD+L-NAME group (Figure 3). Briefly, mice were initially anesthetized using 2-3% isoflurane with oxygen as a carrier gas. Once a deep plane of anesthesia was achieved, mice were placed on a heating pad in a supine position. A nose cone, connected to a breathing circuit and isoflurane anesthesia vaporizer (Dispomed Ltd.), was secured around the muzzle. During the procedure, anesthesia was maintained using 2% isoflurane. Hair on the back of the animal, slightly posterior to the scapulae was removed using a hair remover cream, cleaned with 70% ethanol and 10% betadine. A 1-2 cm incision was made,

and blunt dissection was carried out to create a subcutaneous pocket for subsequent insertion of the osmotic pump. After implanting the osmotic pump, the skin was closed with discontinuous suturing using a 6-0 Polyglycolic Acid (PGA) suture (AD Surgical). Meloxicam (5 mg/Kg) was used for post-operative pain management. Mice were placed in clean cages on a heating pad to recover for 24 hours. Cages were then moved into the animal care facility. Animals were studied 4 weeks after Ang-(1-7) or saline-filled osmotic pump implantation.

2.4. Intraperitoneal glucose tolerance test

An intraperitoneal glucose tolerance test was performed on 6-hour-fasted mice to evaluate the glucose metabolism in the study groups. Briefly, mice from all three groups (Control, HFD+L-NAME+Saline, HFD+L-NAME+Ang-(1-7)) were kept in clean cages without food for 6 hours. During this time, all the mice had access to drinking water *ad libitum*. After 6 hours of fasting, mice were administered glucose (1 g/kg i.p), and blood glucose levels were monitored at 0, 15, 30, 45, 60, 90, and 120-minutes post-glucose administration. Glucose (in)tolerance was determined using temporal analysis of glucose levels plotted against time curves, as previously described by Patel, Mori et al. (Patel, Mori et al. 2016).

2.5. Transthoracic echocardiography and Doppler imaging

To determine the structural and functional changes in all the study groups, transthoracic echocardiography was performed using a VisualSonics Vevo 3100 system at 11 weeks (before administration of Ang-(1-7)/ Saline) as well as 15 weeks (the end of diet) after the initiation of HFD+L-NAME. Structural changes and systolic function of the heart were obtained from short-axis M-mode scans at the midventricular level. For diastolic functions, apical four-chamber views were obtained using pulsed-wave and tissue Doppler imaging at the level of the mitral

valve. All echocardiographic recordings were performed in isoflurane-anesthetized mice. Anesthesia was induced by 4% isoflurane and a surgical plane of anesthesia was continued during echocardiogram acquisition using 1.5-2% of isoflurane. Mice were placed on a warm pad to keep the body temperature around 37°C, and the chest hair was removed using a hair remover cream and the skin was washed with 100% ethanol. Warmed echo gel was placed on the chest, and the mouse heart was imaged with a 30 MHz transducer. Two-dimensional LV long-axis was obtained by placing the transducer along the long-axis of LV and directing to the right of the neck of the mouse. By rotating the transducer 90° clockwise, the LV short-axis view was visualized. Doppler spectra were recorded in an apical 4-chamber view by placing the sample volume at the tip of the mitral valves. Heart rate, left ventricular end-diastolic diameter, left ventricular end-systolic diameter, end-diastolic inter ventricular septal wall thickness, left ventricular end-diastolic posterior wall, left ventricular fractional shortening, left ventricular ejection fraction, peak Doppler blood inflow velocity across the mitral valve during early diastole, peak Doppler blood inflow velocity across the mitral valve during late diastole, isovolumetric relaxation time, peak tissue Doppler of myocardial relaxation velocity at the mitral valve annulus during early diastole and early filling deceleration time was measured. After the scanning was finished, the residual echo gel was removed, and the animal was returned to the cage for recovery. Echo images were downloaded and analyzed using Vevo Lab software.

2.6. Pressure-Volume loop analysis

Although transthoracic echocardiography allows sensitive and sequential analysis of cardiac function, many of the LV functional indices derived from echocardiography are rate and load dependent. To obtain load-independent quantitative information of the cardiac function, LV pressure-volume (PV) relationships were assessed using 1F Pvr-1045 Millar catheter as

previously described (Pacher, Nagayama et al. 2008). Briefly, mice were anesthetized with 2-3% isoflurane in 100% oxygen, hair from the neck and chest area was removed, and the animal was moved to the heating pad, while the isoflurane was kept in 1.5-2%. The temperature and heart rate were monitored during the procedure. An incision was made on the right side of the neck, and a pressure-volume conductance catheter was inserted through the right common carotid artery and advanced retrograde across the aortic valve and into the LV. The PV catheter passes a high-frequency low-amplitude current through two sets of electrodes that are oriented along the longitudinal axis of the LV and simultaneously measure electrical potentials that are proportional to ventricular volume. Using PowerLab 4/30 with LabChart Pro data acquisition system which was connected to the catheter, these signals were converted to instantaneous LV blood volume measurements. Also, integrated into the catheter was a pressure transducer allowing real-time pressure-volume loop generation (Wei, Maslov et al. 2014). The pressure-volume loops were analyzed using LabChart Pro software.

2.7. Histological and immunofluorescence analyses

To visualize structural elements and morphometric measurement of cellular and tissue dimensions, histological staining was performed. Following euthanasia, hearts were collected, washed quickly in phosphate-buffered saline (PBS), and submerged in 1 mol KCl to stop the hearts in diastole. Hearts were then fixed in 10% formalin. Following adequate fixation, tissues were prepared for sectioning and staining in collaboration with the Libin Histopathology Core facilities.

2.7.1. Haematoxylin and Eosin

Haematoxylin and Eosin (H&E) staining was performed to visualize and compare the tissue architecture and inflammatory cell infiltration. Sections of 10 µm were first deparaffinized and were put in haematoxylin for 10 min prior to quick deep in acid alcohol which was followed by washing in PBS and distilled water. Sections were then dipped in the Eosin for 4 min and were washed with ethanol and xylene prior to adding mounting media. Sections were imaged using Olympus VS120 High-Capacity Slide Scanner microscope. Fiji ImageJ software was used to measure the area of LV chamber size for individual images.

2.7.2. Masson Trichrome

Masson Trichrome staining was performed to examine the collagen content. Sections of 10 µm were first deparaffinized and rinsed with distilled water for 10 min. The equal volume of Weigert's iron hematoxylin stock solution A and Weigert's iron hematoxylin stock solution B were prepared and added to the tissue sections which were locally encircled by the PAP-pen. The slides were always covered to prevent drying and incubated for 10 min. Slides were then rinsed with distilled water. A mixture using equal volumes of Phosphomolybdic acid and Phosphotungstic acid solutions was prepared and was then added to the encircled area. Slides were covered and incubated for 15 min. The solution was then discarded, and Aniline blue was added to the slides directly and covered for 20 min. Slides were then rinsed with distilled water, and 1% acetic acid was added for 2 min. Slides were then washed with ethanol and xylene prior to adding mounting media. Sections were imaged using Olympus VS120 High-Capacity Slide Scanner microscope.

2.7.3. Picro Sirius Red

Picro Sirius Red (PSR) staining was performed to examine the collagen content using Confocal Microscopy (Leica TSC SP8) as previously described (Mori, Patel et al. 2014). After deparaffinization, sections were dipped in 0.2% Phosphomolybdic Acid (PMA) for 25 min, and then dipped in PSR solution (containing Picric acid+ 0.1% Sirius Red 9:1) for 90 min. Sections were washed and the mounting media was applied with a coverslip. The sections were then imaged immediately using Leica TSC SP8 Laser Confocal Microscope. Myocardial collagen contents were measured from PSR staining images using Fiji ImageJ software.

2.7.4. Wheat Germ Agglutinin

Wheat germ agglutinin (WGA) was performed to stain the cellular membrane and measure the myocyte cross-sectional area. Following euthanasia, hearts were collected, washed quickly in PBS and 1 mol KCl and snap-frozen in OCT blocks. The OCT blocks were cut in 7 µm thick cryosections and kept at -20°C until the day of staining. Sections were fixed in 4% paraformaldehyde for 20 minutes and washed with PBS at room temperature (RT) for 30 min prior to one-hour incubation with 4% BSA. WGA, Oregon Green® 488 conjugated wheat germ agglutinin (Invitrogen) was added to the sections (200µg/mL in 1.5% BSA) for 25 min at RT. The sections were then washed 3 times with PBS and ProLong Gold antifade reagent with DAPI was added to each section. Coverslips were applied carefully, and the slides were kept in the dark at RT overnight for optimal curing of the sections. Slides were imaged using a line-scanning confocal microscope (Leica TSC SP8). Confocal images were analyzed using the Fiji ImageJ software and the myocyte cross-sectional areas were measured.

2.8. Immunoblot analysis.

2.8.1. Protein Extraction

Proteins were extracted from the snap-frozen LV tissues of the mice using RIPA buffer containing SIGMAFAST protease inhibitor (Millipore Sigma, S8830-2TAB) and PhosSTOP phosphatase inhibitor (Millipore Sigma, 4906837001). Briefly, around 20mg of LV was placed in a microcentrifuge tube containing 400 µl of RIPA buffer and homogenized using TissueLyser LT QIAGEN for 2 min. Samples were kept on ice for 30 min and were vortexed every 10 min during this period. The microcentrifuge tubes were centrifuge at 13200 rpm for 15 min at 4°C. The supernatants, containing proteins, were collected into new tubes and proteins were stored in the -80°C freezer until further experiments.

2.8.2. BCA Protein Assay

To quantify the concentration of the extracted protein samples, a protein assay was performed using the Bio-Rad BCA Protein Assay Kit. Previously extracted protein samples were diluted at 1:10 in RIPA buffer and analyzed in triplicates. The 96-well plate was read on the SpectraMax M2 plate reader. Using the SoftMax Pro 7.0.2 software, the absorbance values were recorded at 700 nm. The average absorbance of the triplicates was calculated for each sample and protein standard. A standard curve was plotted using the linear fit. The concentration of the sample was calculated then multiplied by the dilution factor to determine the concentration of the original protein sample.

2.8.3. Master Mix

A 100 µl master mix solution was prepared in a 1.5 mL microcentrifuge tube as following: 25 µl of NuPAGE LDS Buffer (4X), 10 µl of NuPAGE Reducing Agent (10X), X µl of protein sample, and RIPA buffer.

2.8.4. Gel Electrophoresis

Polyacrylamide gels (8-10%) were used for electrophoresis with SDS Running Buffer. 5 µl of the protein standard (Thermo Fisher ladder) and the calculated volume of master mix (50 µg of protein/well) were pipetted into the desired wells using a loading tip. The gel was run at 50 V for 1 h followed by 100 V for 2 h in 500 mL running buffer (to prepare 1L of running buffer, 30g of Tris base, 144g of glycine, and 10g of SDS was mixed in 1L of distilled H_2O).

2.8.5. Transfer

A 2 L stock solution of transfer buffer (10X) was prepared, for which 60.4g of Tris and 288g of Glycine were dissolved in 2000 mL of distilled H_2O. On the day of the Western Blot experiment, 1 L of transfer buffer (1X) was prepared as following: 100mL of transfer buffer stock solution (10X), 200 mL of methanol, and 700 mL of distilled water which was stored at 4°C until it was cool down and ready for use. The PVDF membrane (6x9 cm) was activated with methanol for 30 seconds before use. The sandwich was made in the following order: a Bio-Rad Mini Trans-Blot Foam Pad, filtered paper, gel, PVDF membrane, filtered paper, and the second Trans-Blot Foam pad. Proteins were transferred at 200 Amp for 2 hours in a Bio-Rad Mini Trans-Blot Cell chamber in the cold room. After transfer, the membrane was blocked in 5% non-fat dry milk in 10 mL of TBST for 1 hour at room temperature. To prepare 500 mL TBST, 500 µl Bio-Rad Tween-20 was added to 500 mL 1X TBS buffer. 1X TBS buffer was prepared from a

10X TBS stock solution. To prepare 2L of 10X TBS buffer, 48g of Tris Base and 176g of NaCl were added to 2L of distilled water, and pH was adjusted to 7.6.

2.8.6. Primary antibody

After one hour of blocking time, the membrane was incubated in the cold room overnight with a primary antibody. The primary antibodies were diluted 1:1000 in 5% non-fat dry milk. The following antibodies were used: pAKT (Thr308; #13038, Cell Signaling Technology), pAKT (Ser473, #4060, Cell Signaling Technology), pERK 1/2 (#9101, Cell Signaling Technology), pp38 MAPK (#9211, Cell Signaling Technology), pAMPKα (#2535, Cell Signaling Technology), pGSK3β (#5558, Cell Signaling Technology), pSTAT3 (Ser727; #9134, Cell Signaling Technology), pSTAT3 (Tyr705; #9145, Cell Signaling Technology), pJAK2 (#3771, Cell Signaling Technology), and pPDH (#ABS204, Sigma-Aldrich). On the following day, the membrane was washed with TBST for 10 min (3 times) at high speed on a platform rocker.

2.8.7. Secondary antibody

The anti-rabbit and anti-mouse (HRP) secondary antibodies (Cell Signaling Technology) were used (1:3000 dilution in 5% non-fat dry milk in TBST). The membrane was incubated with the appropriate secondary antibody at room temperature for 1 hour on the platform rocker at a slow speed. The membrane was washed for 10 minutes (3 times) with TBST on the platform rocker at a high speed.

2.8.8. Imaging

An equal volume of the two reagents (Luminol/Enhancer and Peroxide) of the SuperSignal West Femto chemiluminescence substrate (Thermo Scientific) was added to the conical tube (e.g. 1 mL and 1 mL) and mixed well. The reagent solution was applied evenly over the membrane and the membrane was placed in the dark for 3 min. After 3 minutes of incubation time, the membrane was placed on the tray in the Invitrogen iBright 1500 Imaging System (Invitrogen). The density of the bands was calculated as Volume/Area. The expression of desired phospho proteins was determined relative to total proteins.

2.8.9. Stripping the Membrane

10 mL of Stripping buffer per Membrane was prepared as follows: 1.25 mL of Tris HCl (0.5 M, pH 6.8), 2 mL of 10% SDS, 6.75 of distilled water, and 80 µl of 2-mercaptoethanol. The stripping buffer was placed in an incubator at 50 °C for 10 min before it was added to the Membrane. The Stripping buffer was added to the Membrane and the membrane was incubated on a rocker at slow speed for 40 minutes at 50 °C. The Stripping buffer was removed, and the membrane was rinsed for 2 minutes with tap water and then washed with TBST for 5 minutes on the platform rocker at a high speed (6 times). The membrane was blocked with 5% non-fat dry milk in TBST for one hour. The primary and secondary antibodies were added as described previously.

2.9. Statistical Analysis

All data were presented as mean ± SEM. The data were analyzed blindly, without the knowledge of individual animal's certificate number. Echocardiography and PV loop data were analyzed by at least two individuals. GraphPad Prism 8.0 was used for statistical analyses and for preparing the graphs. For the comparison of three groups, one-way ANOVA was used. Tukey's multiple comparisons test was used as a Post Hoc analysis. All experiments were performed with at least four biological replicates. Statistical significance was recognized when $P < 0.05$.

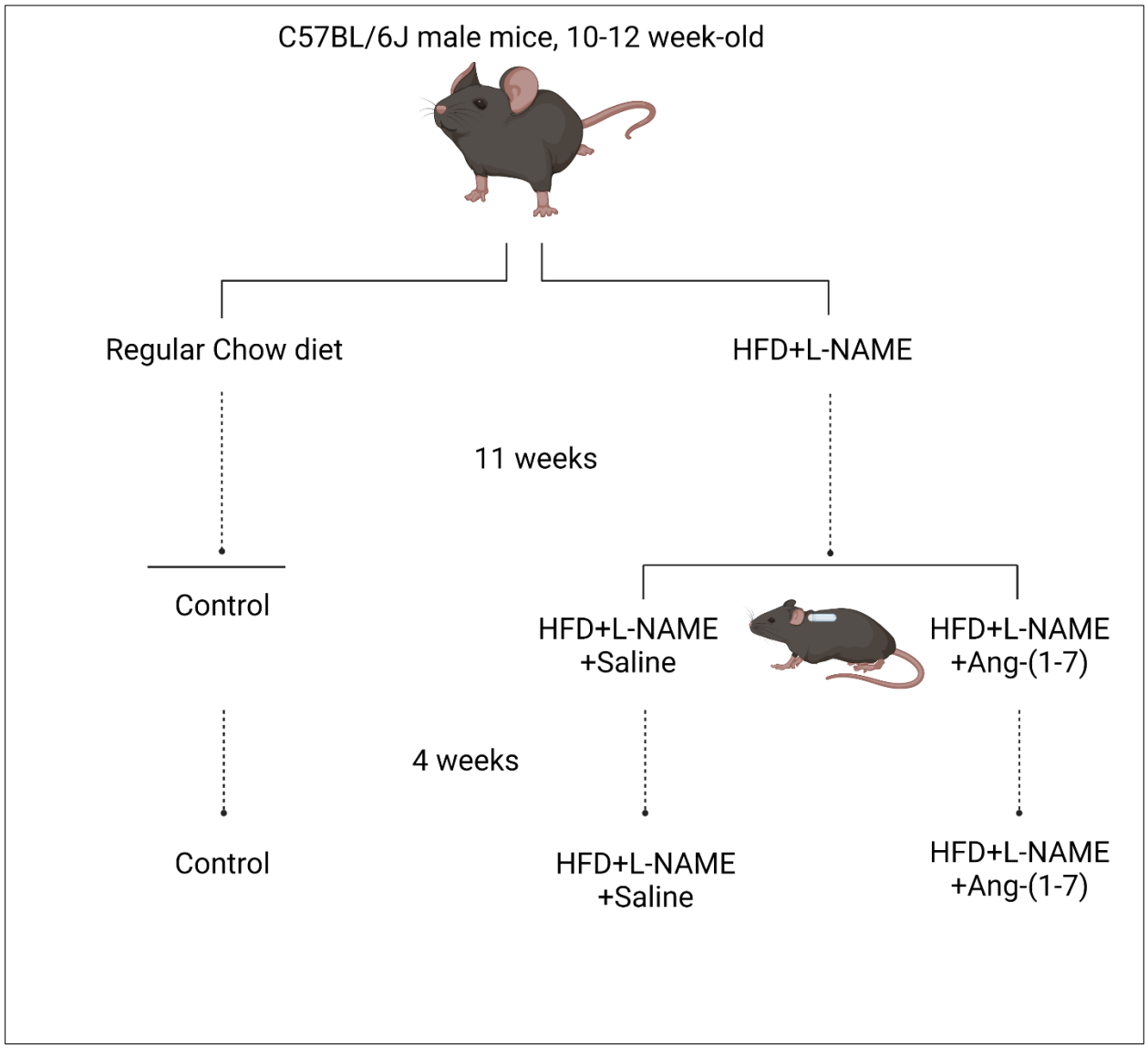

Figure 3. Experimental design. Male mice, 10–12-weeks-old, were divided into two groups to either receive the combination of HFD and L-NAME or regular chow diet for 11 weeks. After 11 weeks, the HFD+L-NAME group was sub-divided into two groups, and micro-osmotic pumps were implanted subcutaneously to either receive Saline as a vehicle or Ang-(1-7) (24µg/Kg/h) for 4 weeks. After the treatment period, structure and function of hearts were examined using transthoracic echocardiography and PV loop analyses. Hearts were collected for further histological and molecular analyses (Created with BioRender.com).

3.1. Angiotensin-(1-7) is not protective against diet-induced obesity.

The bodyweight of all three groups of animals was measured on a weekly basis for 15 weeks after the initiation of HFD+L-NAME treatment. All the mice were given drinking water *ad libitum*. A significant increase in body weight was observed in the HFD+L-NAME group compared to the Control animals that received a regular chow diet. HFD+L-NAME group gained 60.71% increase in body weight over the period of 15 weeks, whereas Control animals gained 39.28% (Figure 4A). Ang-(1-7) administration for 4-weeks did not affect diet-induced obesity; animals in HFD+L-NAME+Ang-(1-7) group gained 75% body weight within a period of 15 weeks of HFD+L-NAME (Figure 4A). In comparison with the Control group, HFD+L-NAME had a 17.38% higher increased in body weight after the period of 15 weeks (Figure 4B), and treatment with Ang-(1-7) did not alter this increase (Figure 4B).

3.2. Effects of Angiotensin-(1-7) treatment on the development of pulmonary edema.

Clinically, HFpEF is often associated with pulmonary hypertension that leads to right ventricular failure in the end-stage HFpEF (Gorter, van Veldhuisen et al. 2018). As a surrogate of pulmonary edema and the development of pulmonary hypertension, we evaluated lung water content. For this purpose, after 15 weeks, the lungs of animals in all three study groups were collected and weighed. The differences between wet and dry lungs were calculated and compared between the groups. There was no significant difference observed in lung water content between the groups (Control= 161.3±4.91; HFD+L-NAME= 166.3±3.66; HFD+L-NAME+Ang-(1-7) =154.1±5.12). Albeit 4-weeks of Ang-(1-7) administration resulted in a non-

significant decrease in lung water content (P=0.16), which can be indicative of modest protective effects of Ang-(1-7) against the development of pulmonary hypertension and edema (Figure 4C).

3.3. Effects of Angiotensin-(1-7) on glucose tolerance.

Increased glucose intolerance, hyperglycemia, and metabolic dysfunction are the common comorbidities observed in patients with HFpEF. 15 weeks of HFD+L-NAME led to a significant increase in glucose intolerance (35.22% increase compared to Control) which was observed by analyzing the area under the curve. Ang-(1-7) treatment mildly reduced the glucose intolerance level (11.94%) (Figure 4E).

3.4. Angiotensin-(1-7) improves LV systolic function and Ejection Fraction.

To confirm that our study model mimics the clinical phenotype of HFpEF, systolic function of LV was examined using invasive and non-invasive techniques. Ejection fraction (EF) (Control= 52.36±1.42; HFD+L-NAME= 52.16±1.71; HFD+L-NAME+Ang-(1-7)= 53.82±1.60), fractional shortening (FS) (Control= 24.92±0.86; HFD+L-NAME= 25.64±1.11; HFD+L-NAME+Ang-(1-7)= 26.08± 0.87), and ejection time (ET) (Control= 53.75±1.43; HFD+L-NAME= 51.76±1.52; HFD+L-NAME+Ang-(1-7)= 53.72±1.38) were preserved as evident from data analysed using the M-mode and Doppler echocardiography images (Figure 5A, 5B, 5C, respectively). Similarly, preserved EF was detected using PV loops (Control= 60.51± 4.86; HFD+L-NAME= 60.32±2.53; HFD+L-NAME+Ang-(1-7) = 71.42±5.35) (Figure 7A). Interestingly, PV loops data indicated that Ang-(1-7) treatment can result in improvement of EF (16.58% compared to HFD+L-NAME; 16.53% compared to Control) (Figure 7A). Isovolumetric contraction time (IVCT) was reduced significantly in HFD+L-NAME group (25.28% compared to Control), which was reversed after 4-weeks Ang-(1-7) treatment (25.51% compared to

HFD+L-NAME) (Figure 5D). End systolic pressure volume relationship (ESPVR) did not have significant changes in the three study groups (Control= 2.34±0.59; HFD+L-NAME= 2.96±0.43; HFD+L-NAME+Ang-(1-7) = 2.05±0.57) (Figure 7B).

3.5. Angiotensin-(1-7) recovers both active and passive relaxation.

Different parameters of diastolic dysfunction were examined using pulse wave Doppler, tissue Doppler, and PV loop analysis. A significant increase in isovolumetric relaxation time (IVRT) was observed in HFD+L-NAME compared to Control (15.60%) which was reversed with 4-weeks Ang-(1-7) treatment (13.34%) (P= 0.056) (Figure 6A). Impaired relaxation was confirmed with PV loop analysis and the Tau value. A significant increase of Tau value was detected in the HFD+L-NAME group compared to Control (22.43%) which was recovered with 4 weeks of Ang-(1-7) treatment (22.16%) (Figure 7D). Alteration in the passive filling of LV can also lead to diastolic dysfunction. Looking at the early to the late filing of LV, the ratio of early to the late filing of LV (E/A) was not altered significantly after 15 weeks of HFD+L-NAME (Control= 1.54±0.05; HFD+L-NAME= 1.43±0.03; HFD+L-NAME+Ang-(1-7) = 1.63±0.10) (Figure 6B). However, E/A ratio was mildly improved after 4-weeks Ang-(1-7) treatment (13.07%) (P=0.10) (Figure 6B). To have a better understanding of diastolic function, the ratio of the early filling of pulse wave Doppler (E) to the early filling in tissue doppler (E') was obtained. A significant increase in the E/E' was demonstrated in HFD+L-NAME compared to Controls (27.51%) which was slightly, although non-significantly, improved with 4 weeks of Ang-(1-7) treatment (5.21%) (Figure 6C). Impairment of LV filling was also detected using PV loop data. Although a rise was demonstrated in the end-diastolic pressure-volume relationship (EDPVR) of HFD+L-NAME compared with Control (18%), this enhancement was not significant and was slightly improved with 4 weeks Ang-(1-7) treatment (15.73%) (Figure 7E). A significant

increase in end-diastolic pressure (LVEDP) was also detected in the HFD+L-NAME group (72.43%) which was restored with 4-weeks Ang-(1-7) treatment (63.78%) (Figure 7C).

3.6. Angiotensin-(1-7) reduces the level of fibrosis.

PSR and Masson Trichrome staining were used to detect the levels of interstitial fibrosis (Figure 8A, 8B). 20 different Confocal images from PSR staining were chosen from a different area of LV of each heart, and the percentage of fibrosis was detected using Fiji ImageJ. The PSR staining exhibited a modest increase in the level of fibrosis in the HFD+L-NAME group compared to the Control (16.20%); interstitial fibrosis was moderately reduced with Ang-(1-7) treatment (59.73%). However, the changes in collagen content were not significant (P=0.16) (Figure 8B). In line with PSR staining, Masson Trichrome staining did not detect any changes in fibrosis levels in different study groups (Figure 8A).

3.7. Angiotensin-(1-7) partially improves cardiac hypertrophy.

M-Mode echocardiography, Western blotting, H&E staining, and WGA staining were used to examine the changes in LV structure. Analysis of M-Mode echocardiography images showed a decrease in LV end-diastolic dimension (LVEDD) and LV end-systolic dimension (LVESD) in the HFD+L-NAME group compared to Control (6.97% and 14.16% respectively). A 4-weeks treatment with Ang-(1-7) increased the LVEDD by 4.18% and LVESD by 2.45% which were not significant (Figure 9A, 9B). Furthermore, a significant increase was detected in LV posterior wall thickness in diastole (LVPWd) in HFD+L-NAME (13.33%) which was slightly reduced after 4 weeks of treatment with Ang-(1-7) (8.28%) (Figure 9C). These changes are indicatives of the development of cardiac hypertrophy. To confirm the decrease in chamber size, H&E staining was used. 15 weeks of HFD+L-NAME reduced the LV chamber size by 50.03% compared to the

Control group and Ang-(1-7) treatment mildly reversed this reduction by 40.24% (Figure 10A). Moreover, WGA staining was used to measure cardiomyocytes' area. The cardiomyocyte cross-sectional area was measured from 35 different cardiomyocytes in different regions of LV. A significant increase was observed in cardiomyocytes of the HFD+L-NAME group compared to Control (50.08%), which was slightly reduced after 4-weeks treatment of Ang-(1-7) (26.02%) (Figure 10B). To further evaluate different molecular pathways related to hypertrophy, immunoblotting analysis was performed. The expression levels of phosphorylated AKT, mTOR, AMPK, GSK3β, MAPK ERK 1/2, MAPK p38, JAK2, and STAT3 were detected. Phosphorylation of AKT at threonine residue (Thr308) (Control= 1.03±0.15; HFD+L-NAME= 1.11±0.16; HFD+L-NAME+Ang-(1-7) = 0.92±0.08) and serine residue (Ser473) (Control= 1.06±0.19; HFD+L-NAME= 1.02±0.25; HFD+L-NAME+Ang-(1-7) = 1.29±0.11) did not have significant change after 15 weeks of HFD+L-NAME and the phosphorylation of this protein did not alter with 4 weeks of Ang-(1-7) treatment(Figure 11A). The expression level of mTOR was tested at serine residue (Ser2448) which was similar for all three groups of study (Control= 1.00±0.02; HFD+L-NAME= 1.02±0.20; HFD+L-NAME+Ang-(1-7) = 0.96±0.13) (Figure 11C). The phosphorylation level of ERK 1/2 at Threonine and Tyrosine residues (Thr 202, Tyr 204) did not have a significant increase after 15 weeks of HFD+L-NAME (28.74% compared to the Control), however, the expression level of this protein was significantly reduced after 4 weeks of Ang-(1-7) treatment (73.35%) (Figure 12A). The phosphorylation level of p38 MAPK at Threonine and Tyrosine residues (Thr180 and Tyr182) did not have significant changes in the three groups (Control= 0.82±0.19; HFD+L-NAME= 0.66±0.12; HFD+L-NAME+Ang-(1-7) = 0.55±0.26) (Figure 12B). Phosphorylation of GSK3β at serine residue (Ser 9) had a considerable increase of 33.49% (P=0.06) after 15 weeks of HFD+L-NAME which was slightly reduced with

Ang-(1-7) treatment (10.45%) (Figure 12C). The expression level of phosphorylated STAT3 (Ser 727) was slightly increased by 13.58% in HFD+L-NAME compared to Control, which was reduced by 31.90% after 4-weeks treatment with Ang-(1-7), however, these changes were not significant (Figure 13A). The expression level of phosphorylated Jak2 (Tyr 1007/1008) did not alter after 15 weeks of HFD+L-NAME and remained the same with Ang-(1-7) treatment (Control= 0.999±0.003; HFD+L-NAME= 1.011±0.40; HFD+L-NAME+Ang-(1-7) = 1.062±0.101) (Figure 13C). The expression level of AMPK at phosphorylated level (Thr 172) had a significant decrease after 15 weeks of HFD+L-NAME (48.12%), which was moderately increased by 24.67% with 4 weeks of Ang-(1-7) treatment (Figure 14A). Phosphorylation of PDH at Serine residue (Ser 293) had a significant increase of 38.73% in HFD+L-NAME and 4-weeks treatment with Ang-(1-7) did not alter this enhancement (Figure 14B).

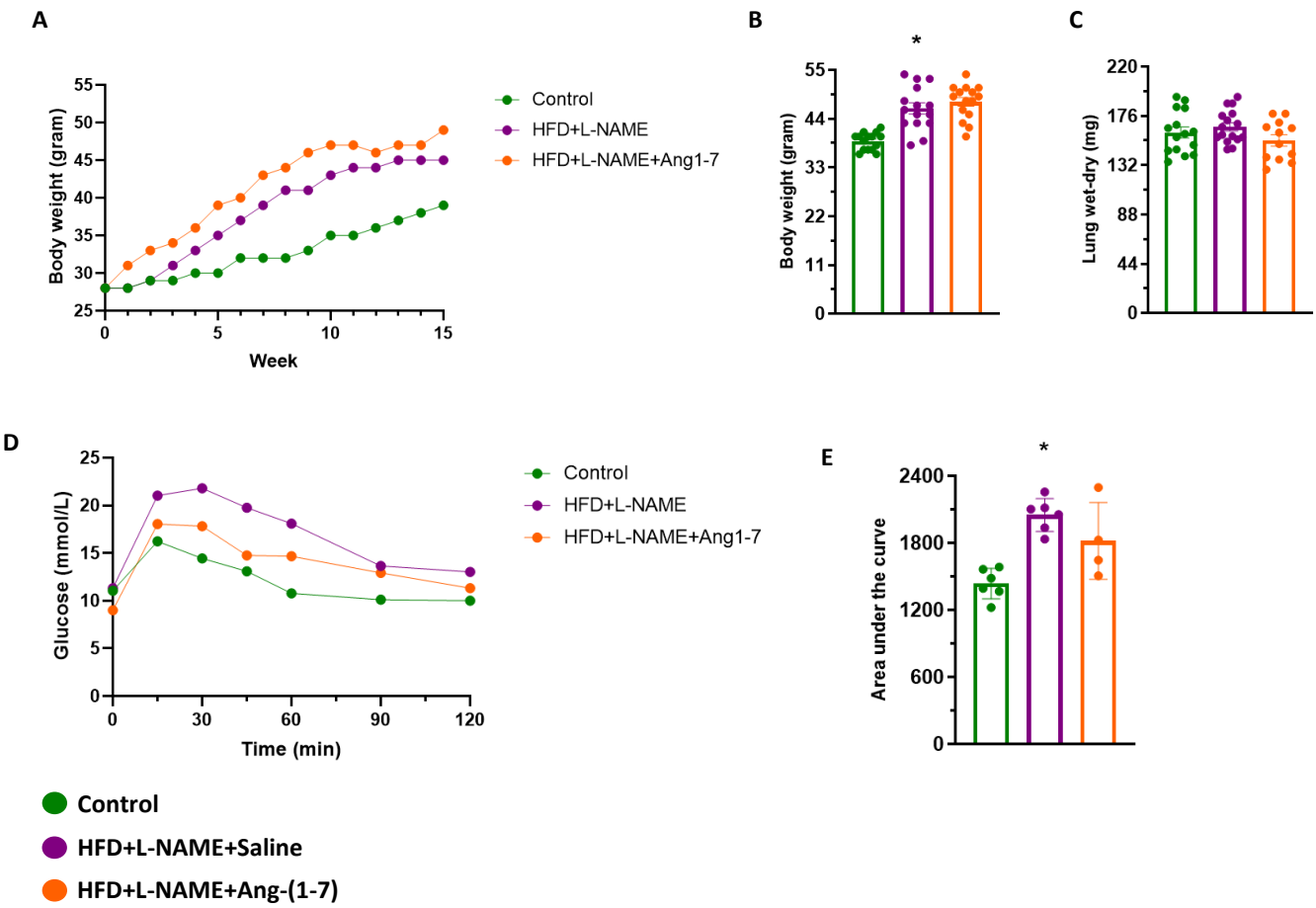

Figure 4. Different comorbidities associated with the preclinical model of HFpEF. (A) Bodyweight of animals in Control, HFD+L-NAME+Saline, and HFD+L-NAME+Ang-(1-7) was measured weekly. (B) A significant increase was observed in the bodyweight of animals after 15 weeks of HFD+L-NAME. A 4-weeks treatment with Ang-(1-7) did not reduce the body weight (n=15). (C) Neither 15 weeks of HFD+L-NAME, nor 4 weeks treatment with Ang-(1-7) affected the lung water content (differences between wet and dry lung weights) (n=15). (D) Increased level of blood glucose was observed in HFD+L-NAME which was moderately reduced with Ang-(1-7) treatment (n=4-6). (E) Area under the curve derived from the Glucose tolerance test indicated a significant glucose intolerance in the HFD+L-NAME group compared to Control, which was non-significantly reduced with 4-weeks Ang-(1-7) treatment. * Represents p-value < 0.05 between Control and HFD+ L-NAME groups.

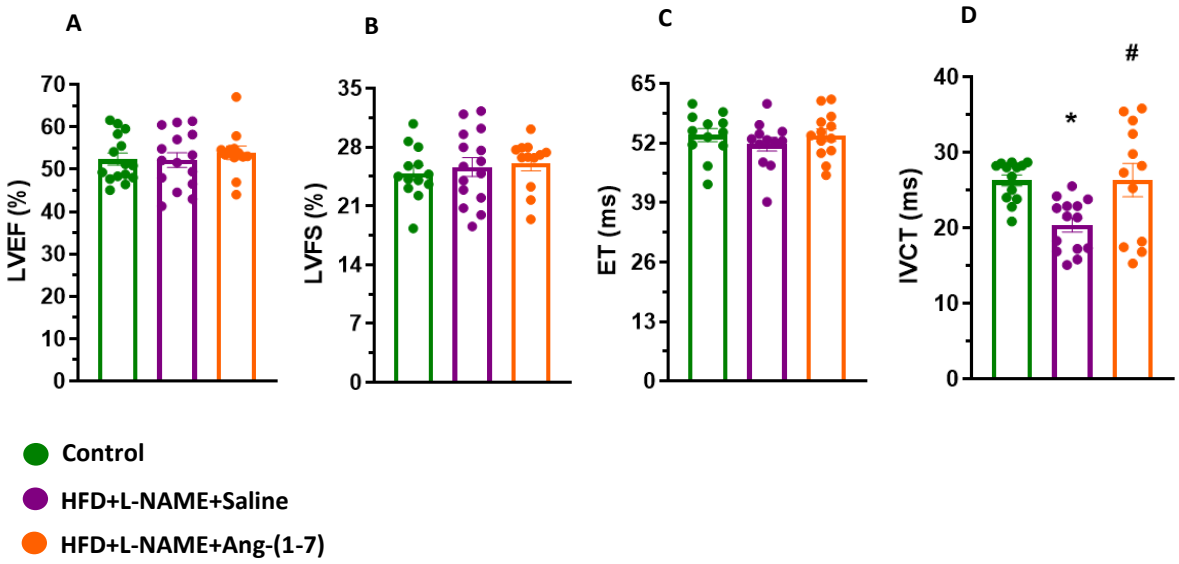

Figure 5. Systolic function remained preserved in the murine "two-hit" model. Systolic function was obtained by pulsed-wave Doppler analyses. (A) Ejection fraction (EF) remained preserved after 15 weeks of HFD+L-NAME; 4 weeks of treatment with Ang-(1-7) did not alter the EF. (B) Similar to EF, fractional shortening (FS) remained unaffected between all the study groups. (C) Ejection time (ET) was not altered with HFD+L-NAME as well as with Ang-(1-7). (D) A significant decrease was observed in isovolumetric contraction time (IVCT) after 15 weeks of HFD+L-NAME; 4-weeks of treatment with Ang-(1-7) restored the IVCT. * Represents p-value < 0.05 between Control and HFD+L-NAME groups. # Represents p-value < 0.05 between HFD+ L-NAME and HFD+ L-NAME +Ang 1-7 groups (n=12-15).

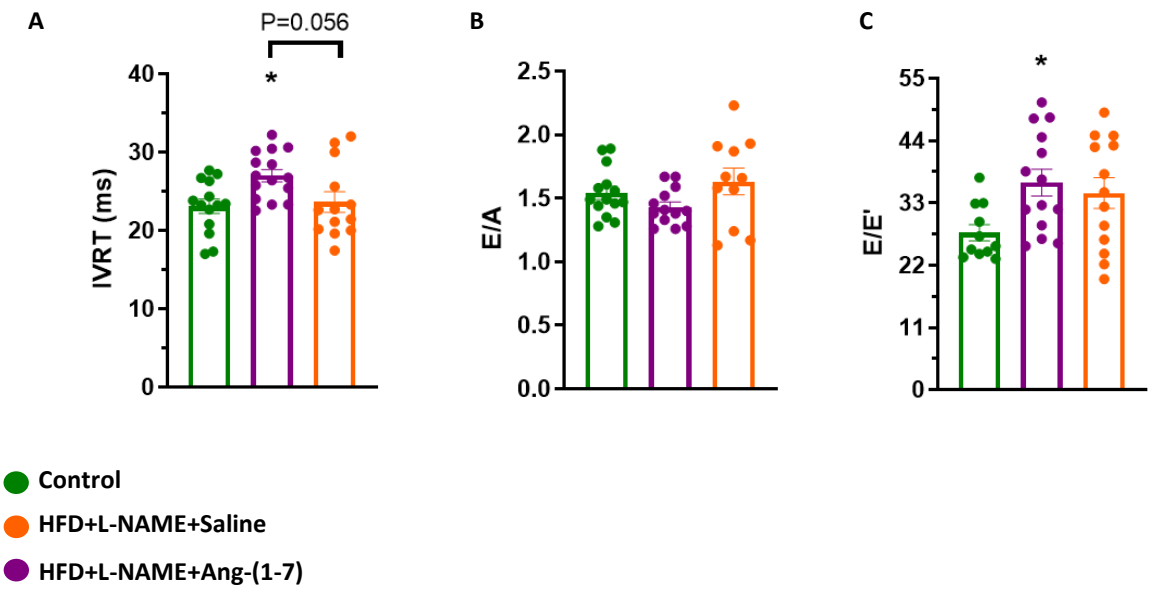

Figure 6. Ang-(1-7) treatment improved the diastolic function, which was impaired in HFD+L-NAME. Diastolic function was evaluated using pulsed-wave Doppler and tissue Doppler analyses. (A) Isovolumetric relaxation time (IVRT) was increased after 15 weeks of HFD+L-NAME and was reversed with Ang-(1-7) treatment. (B) Ratio of early to late filling (E/A) of LV did not show any difference between all the study groups. (C) Ratio of late filling in pulsed-wave Doppler to the late filling in tissue Doppler (E/E') is considered a sensitive index of diastolic function. E/E' was markedly increased in the HFD+L-NAME group compared to Control group. Ang-(1-7) treatment modestly, albeit non-significantly reduced E/E'. * Represents p-value < 0.05 between Control and HFD+L-NAME groups (n=12-15).

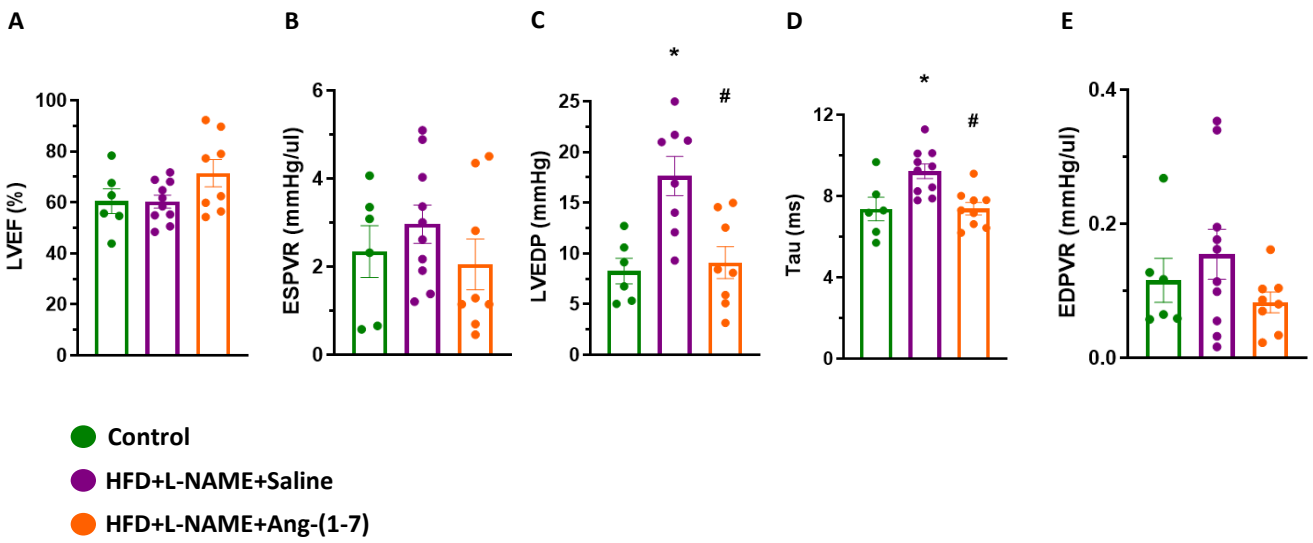

Figure 7. Hemodynamic assessment using Pressure-Volume loop analysis. Various parameters related to systolic and diastolic function were obtained using PV loop analyses. (A) Ejection fraction (EF) was preserved after 15 weeks of HFD+L-NAME; Ang-(1-7) treatment resulted in a modest, albeit non-significant, increase in EF. (B) End systolic pressure-volume relationship (ESPVR), a measure of rate-independent cardiac contractility, was not altered significantly with 15 weeks of HFD+L-NAME treatment compared to the Control group; Ang-(1-7) did not affect the ESPVR significantly. (C) End diastolic pressure showed a significant increase in the HFD+L-NAME group compared to the Control group. Moreover, 4-weeks treatment with Ang-(1-7) attenuated increased LVEDP. (D) 15 weeks of HFD+L-NAME challenge resulted in a significant increase of Tau value, which was reversed with 4-weeks of Ang-(1-7) treatment. (E) End diastolic pressure-volume relationship (EDPVR), a rate-independent measure of cardiac muscle stiffness did not show any significant difference between all of the study groups. * Represents p-value < 0.05 between Control and HFD+L-NAME group. # Represents p-value < 0.05 between HFD+L-NAME and HFD+L-NAME +Ang-(1-7) group (n=6-8).

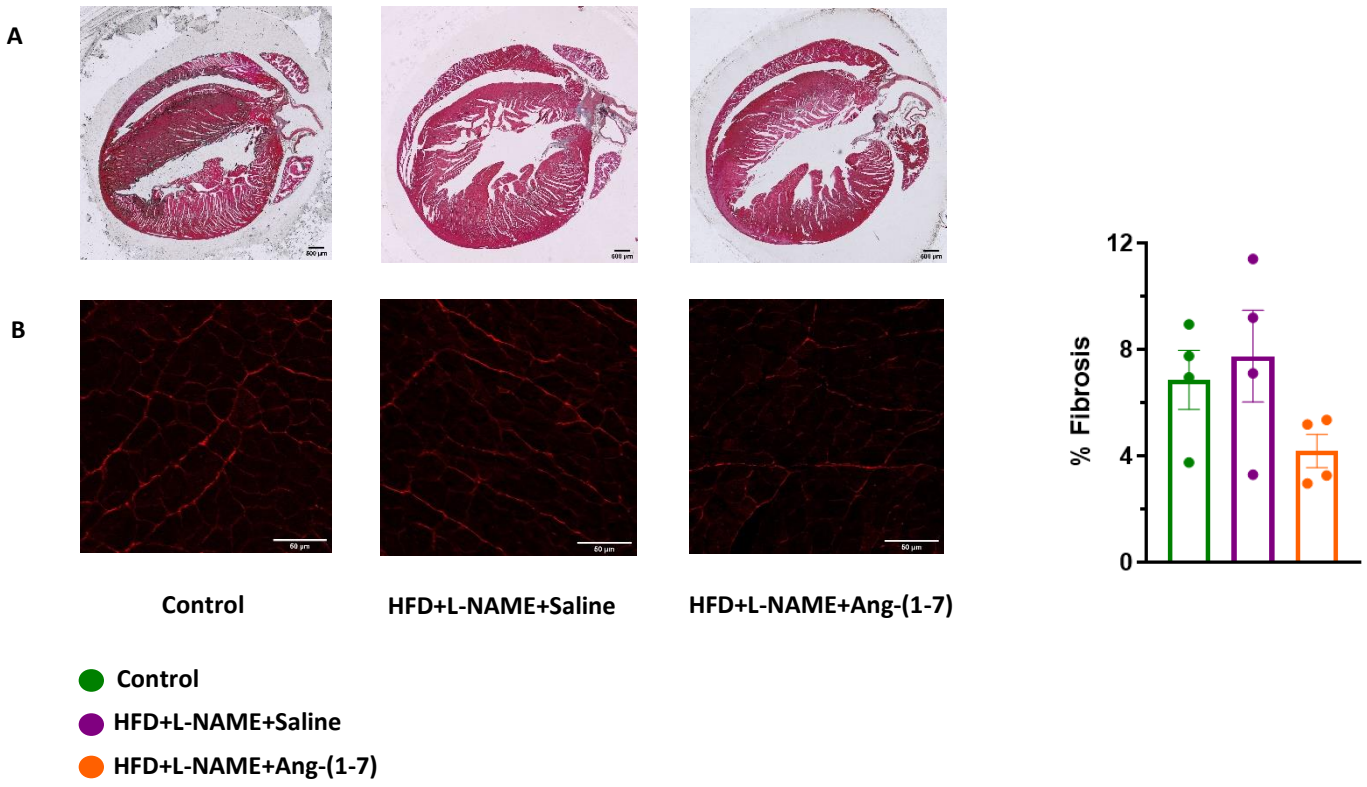

Figure 8. Effects of Ang-(1-7) treatment on cardiac fibrosis. Using bright-field and confocal microscopy imaging techniques, interstitial fibrosis was detected. (A) Masson Trichrome staining represented the absence of interstitial fibrosis in all of the study groups. (B) PSR staining images and their quantification corroborated the lack of interstitial fibrosis in all of the study groups (n=4).

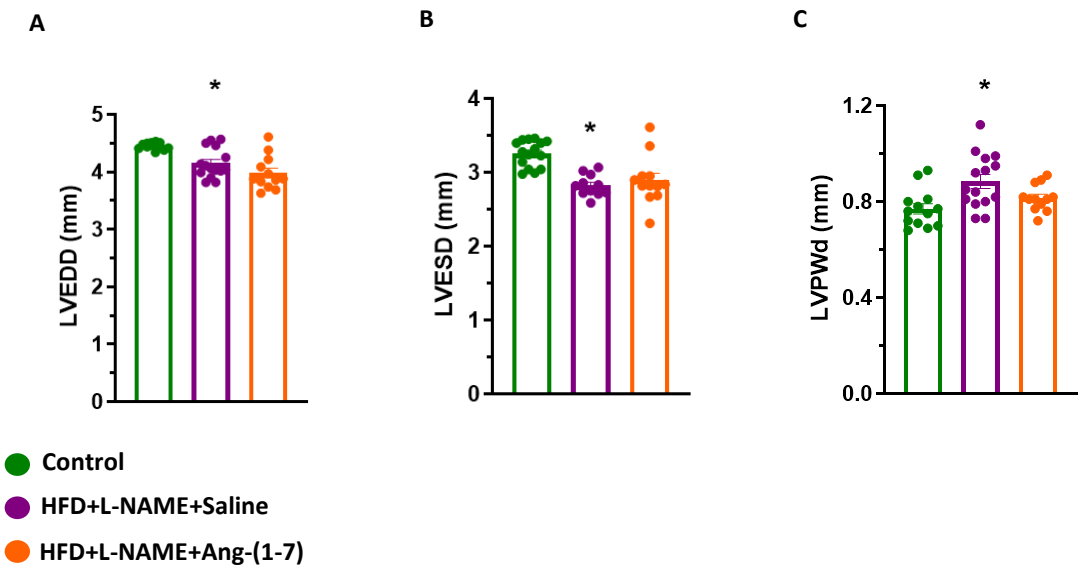

Figure 9. Effects of Ang-(1-7) on cardiac remodeling. M-mode images of transthoracic echocardiography were analyzed to evaluate LV structural changes. (A) LV end-diastolic dimension (LVEDD) was reduced significantly after 15 weeks of HFD+L-NAME. (B) LV end-systolic dimension (LVESD) was also significantly decreased with HFD+L-NAME. 4-weeks treatment with Ang-(1-7) did not reverse the changes in LVEDD and LVESD. (C) LV posterior wall thickness in diastole (LVPWd), a measure of cardiac hypertrophy, was significantly increased after 15 weeks of HFD+L-NAME, which was not improved with Ang-(1-7) treatment. * Represents p-value < 0.05 between Control and HFD+L-NAME groups (n=12-15).

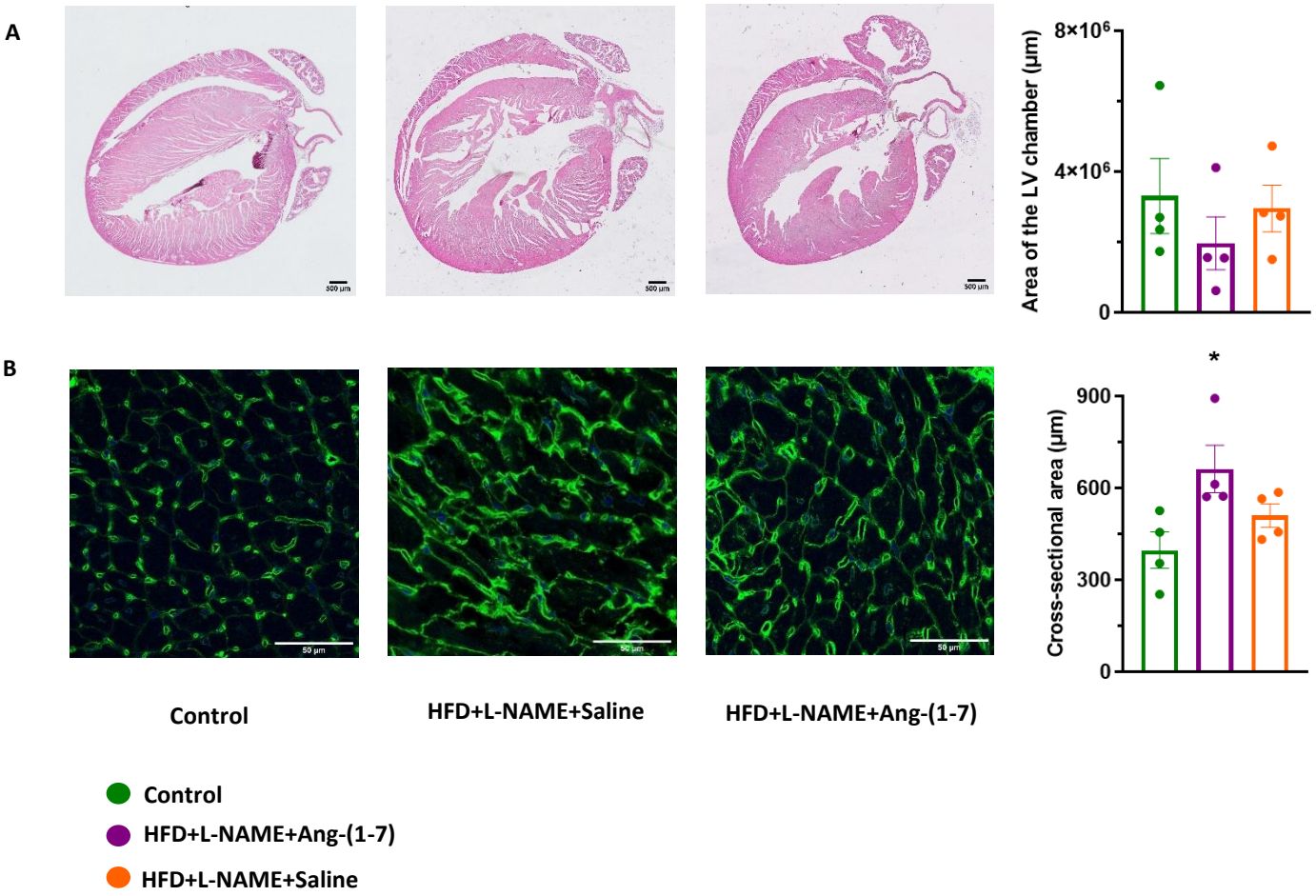

Figure 10. Effects of Ang-(1-7) on cardiac hypertrophy and cardiomyocytes cross-sectional area. (A) H&E staining images and quantification of LV chamber area of heart sections indicated unchanged LV chamber size along with thickened LV wall, representing LV hypertrophy in the HFD+L-NAME group. Ang-(1-7) treatment reduced cardiac hypertrophy as shown in representative H&E staining image (n=4). (B) Using confocal microscopy images, cardiomyocytes' cross-sectional area was measured**.** The cross-sectional area of LV cardiomyocytes significantly increased with 15 weeks of HFD+L-NAME, whereas the 4-weeks treatment with Ang-(1-7) reduced it. However, the changes in the cardiomyocyte cross-sectional area were not significant after 4-weeks Ang-(1-7) treatment. * Represents p-value < 0.05 between Control and HFD+L-NAME groups (n=4).

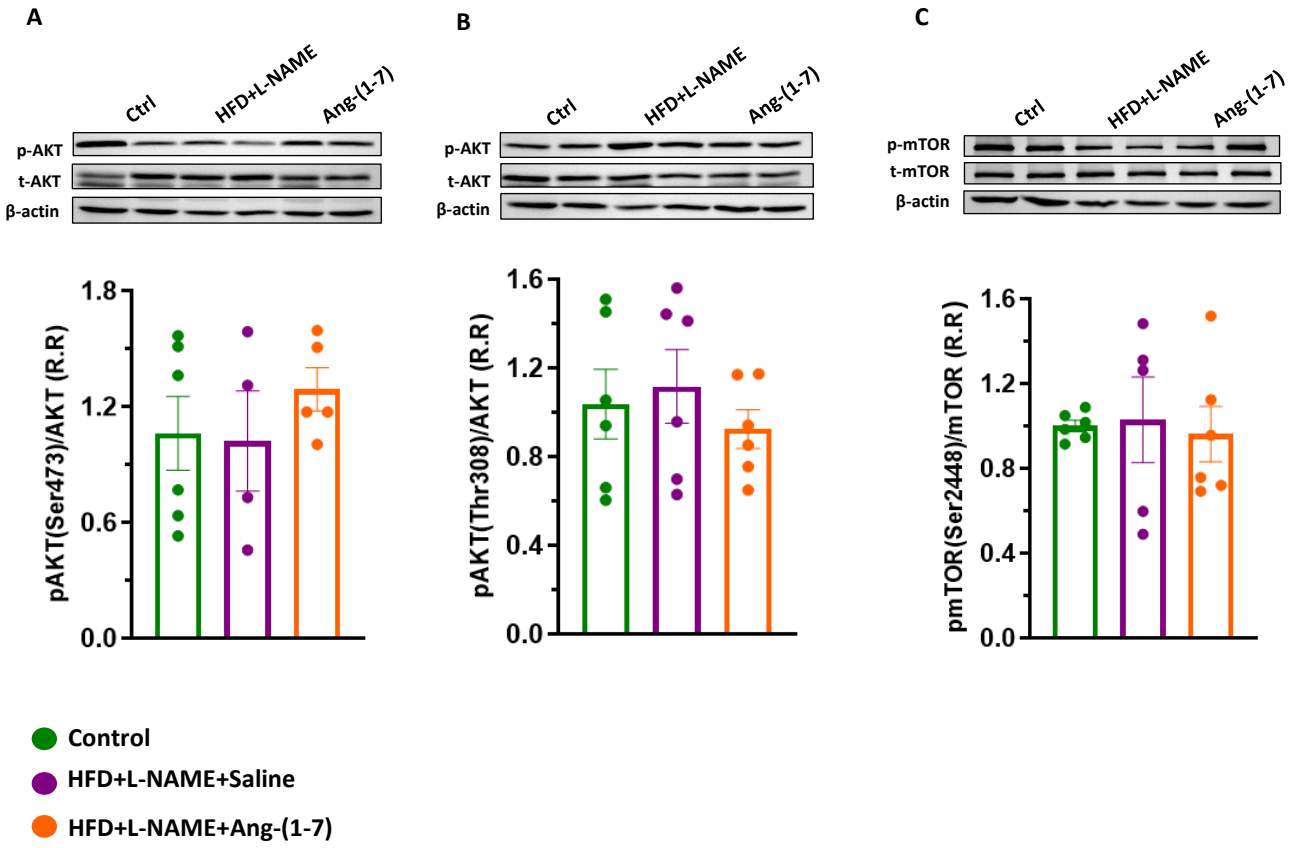

Figure 11. Western blot analyses of PI3K/AKT/mTOR signaling pathway. (A-C) The expression level of pAKT at Serine residue, Ser473 (A) and Threonine residue, Thr308 (B) and pmTOR at Serine residue, Ser2448 (C) were not altered after 15 weeks of HFD+L-NAME as well as after 4-weeks treatment with Ang-(1-7) (n=4-6).

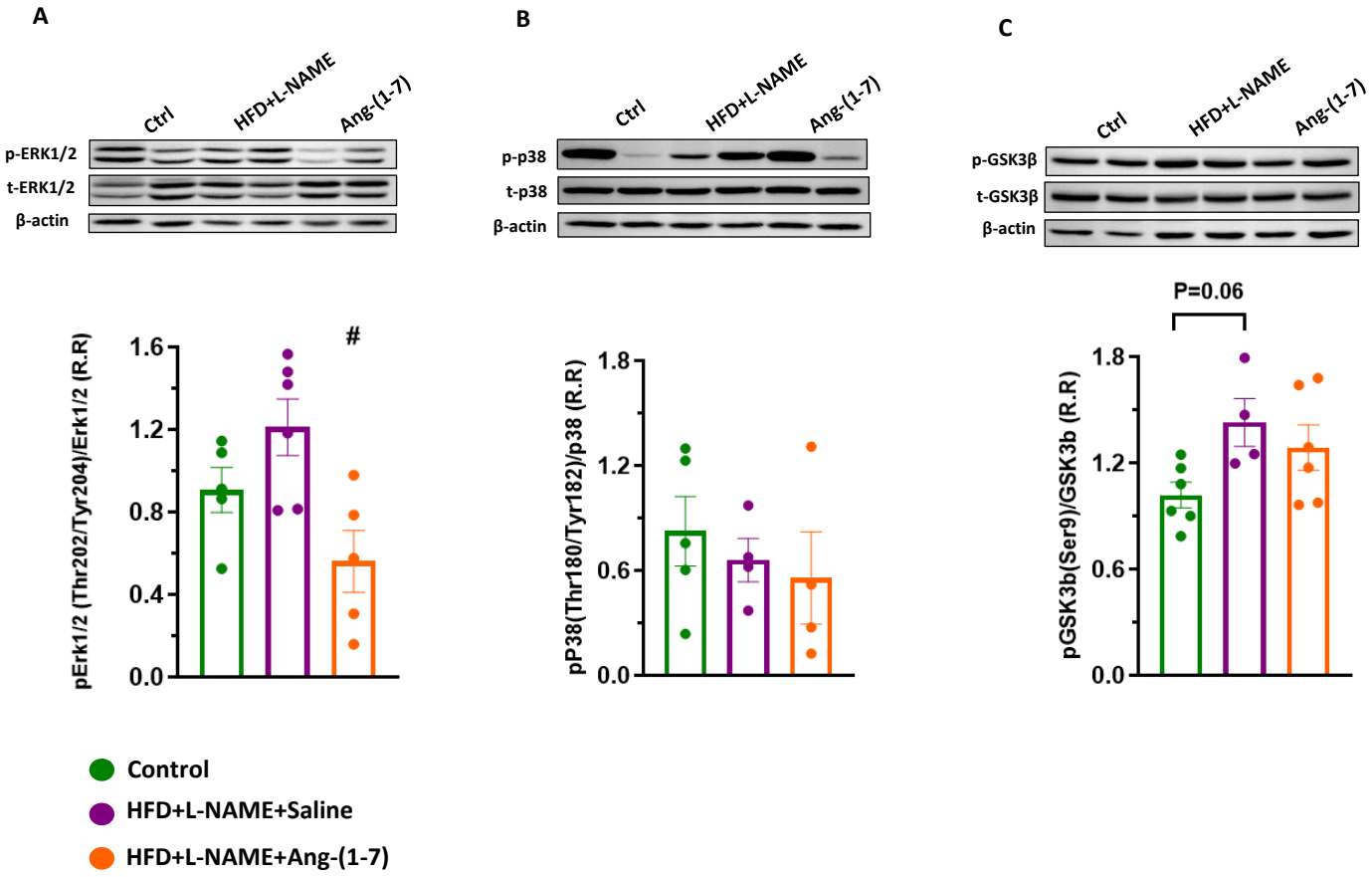

Figure 12. Effects of Ang-(1-7) on ERK1/2 and p38 MAPKs as well as pGSK3β signaling pathways. (A) Phosphorylation of ERK1/2 at Threonine and Tyrosine residues (Thr202/Tyr204) increased, albeit non-significantly, after 15 weeks of HFD+L-NAME; Ang-(1-7) treatment attenuated the phosphorylation and activation of ERK1/2. (B) Expression levels of phosphorylated p38 MAPK did not show any changes after 15 weeks of HFD+L-NAME and Ang-(1-7) treatment. (C) Phosphorylation of GSK3β at Serine residue (Ser9) increased after 15 weeks of HFD+L-NAME and Ang-(1-7) treatment slightly and non-significantly reduced the expression level of pGSK3β. # Represents p-value < 0.05 between HFD+L-NAME and HFD+L-NAME +Ang 1-7 groups (n=4-6).

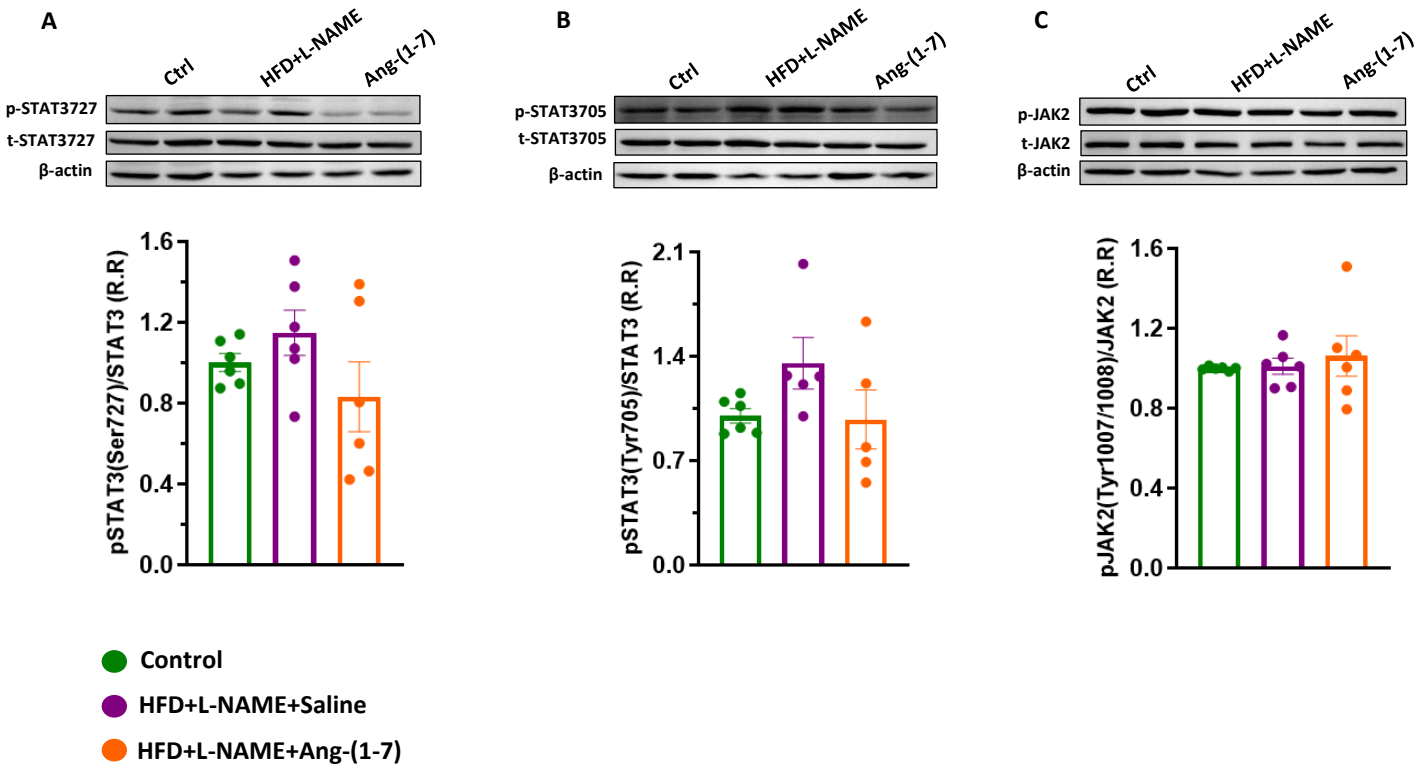

Figure 13. Effects of Ang-(1-7) on JAK/STAT signaling pathway. (A) The expression level of pSTAT3 at Serine residue (Ser727) did not show any significant change after 15 weeks of HFD+L-NAME. Ang-(1-7) did not change the expression level of this protein significantly. (B) Phosphorylation level of STAT3 at Tyrosine residue (Tyr705) showed a non-significant increase with 15 weeks of HFD+L-NAME; 4-weeks treatment with Ang-(1-7) mitigated the phosphorylation of STAT3 at Tyr705. (C) Expression level of pJAK2 was not altered either with 15 weeks of HFD+L-NAME or 4 weeks of treatment with Ang-(1-7) (n=4-6).

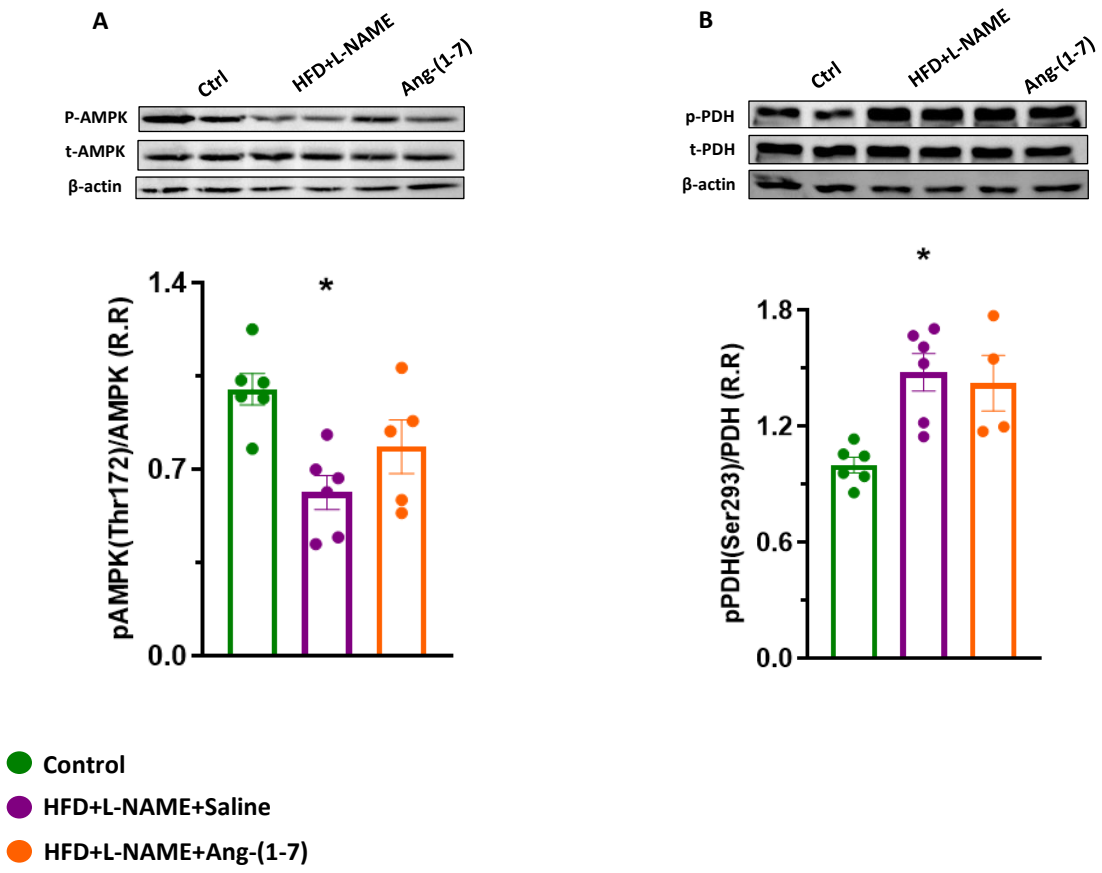

Figure 14. Effects of Ang-(1-7) on metabolic modulator signaling pathways. (A) Expression levels of pAMPK at Threonine residue (Thr172) were significantly decreased after 15 weeks of HFD+L-NAME. Treatment with Ang-(1-7) partially restored the phosphorylation status of AMPK, though this change did not achieve statistical significance. (B) Phosphorylation levels of PDH at Serine residue (Ser293), which results in inactivation of PDH, showed a significant increase after 15 weeks of HFD+L-NAME. However, 4-weeks treatment with Ang-(1-7) did not show any effects on phosphorylation of PDH. * Represents p-value < 0.05 between Control and HFD+ L-NAME groups (n=4-6).

Chapter 4: Discussion, Conclusion, Limitation and Future Direction

4.1. Discussion

The main aims of this study were to determine 1) the effects of Ang-(1-7) on comorbidities associated with HFpEF in a murine model; 2) the effect of Ang-(1-7) on HFpEF associated cardiac remodeling and diastolic dysfunction; and 3) the effect of Ang-(1-7) on various molecular pathways related to hypertrophy and metabolic dysfunction.

Our first research goal was to generate the HFpEF murine model: we used the "two-hit" HFpEF mouse model that was recently developed by Schiattarella et al. (Schiattarella, Altamirano et al. 2019). It has been demonstrated that the combination of HFD and L-NAME led to hypertension, one of the most common comorbidities observed clinically in patients with the HFpEF, as well as a metabolic dysfunction, as evident by increased body weight and glucose intolerance. Furthermore, the combination of HFD and L-NAME lead to pulmonary congestion, exercise intolerance, and a robust increase in left ventricular filling pressure, making it a valuable murine model of HFpEF that mimics many of the clinical observations from patients with HFpEF (Schiattarella, Altamirano et al. 2019). Therefore, to evaluate the effect of Ang-(1-7) in HFpEF, we subjected 10-12-weeks-old wild-type male mice to 15 weeks of HFD-feeding (containing 60% Kcal of fat) along with L-NAME (0.5g/L) in drinking water. The Control group received a regular chow diet and tap water for the same duration. Body weight was measured once a week. A significant increase in body weight was observed with HFD+L-NAME, whereas four weeks of Ang-(1-7) treatment did not affect the body weight. An increase in Ang-(1-7) levels has previously been shown to improve insulin sensitivity and glucose as well as lipid metabolism (Santos, Braga et al. 2010, Vargas-Castillo, Tobon-Cornejo et al. 2020).

Furthermore, it has been determined that Ang-(1-7) treatment reduced HFD-induced obesity by increasing thermogenesis (Morimoto, Mori et al. 2018, Vargas-Castillo, Tobon-Cornejo et al. 2020). Although the exact mechanism of anti-obesity effects of Ang-(1-7) is not known, Ang-(1-7) had been suggested to stimulate browning of white adipose tissue (WAT) through NO via the Mas receptor pathway and stimulates energy expenditure and enhance mitochondrial respiration (Vargas-Castillo, Tobon-Cornejo et al. 2020). Furthermore, it was indicated that the overexpression of Ang-(1-7) induces resistance to obesity (Vargas-Castillo, Tobon-Cornejo et al. 2020). Consequently, the lack of effects of Ang-(1-7) on obesity in our model can be attributed to the inhibition of eNOS, and NO production, by L-NAME.

Activation of Ang-(1-7)/MasR pathways promotes an improvement in insulin sensitivity, glucose, and lipid metabolism (Santos, Braga et al. 2010). Furthermore, Ang-(1-7)/MasR increased mitochondrial respiration in vitro and in vivo (Morimoto, Mori et al. 2018, Vargas-Castillo, Tobon-Cornejo et al. 2020). 15 weeks of HFD+L-NAME resulted in a significantly increased glucose intolerance, which was moderately reduced with Ang-(1-7) treatment. However, the metabolic changes in response to Ang-(1-7) treatment was not significant, which can be due to the loss of NO-dependent effects of Ang-(1-7) in our murine model. Furthermore, pulmonary dysfunction is a common comorbidity observed in end-stage heart failure. A key symptom that is indicative of pulmonary dysfunction in heart failure is pulmonary edema (Papinska, Soto et al. 2016). To understand if HFD+L-NAME leads to pulmonary edema, differences in the wet and dry lungs were calculated. Interestingly, we did not observe any differences in lung water content in any of our study groups. Lack of pulmonary edema in our murine model may be due to an early stage of heart failure. Development of pulmonary edema

may require further extension of HFD+L-NAME treatment which would result in advanced heart failure and pulmonary dysfunction.

The two major characteristics that define HFpEF in patients are diastolic dysfunction and preserved ejection fraction that, in most cases, does not translate to reduced ejection fraction. Using M-mode echocardiography, preserved systolic function was validated by evaluation of LVEF and LVFS. Furthermore, PV loop analysis corroborated the preserved ejection fraction in all of the study groups. Compared to HFrEF patients, patients with HFpEF exhibit increased LV wall thickness as well as the ratio of LV wall thickness to LV chamber size (Borlaug and Redfield 2011). The concentric remodeling in HFpEF and associated increased contractility leads to preserved systolic function and impaired diastolic function. To further evaluate the diastolic function, pulsed wave Doppler imaging, tissue Doppler imaging of the papillary muscles, and pressure-volume relationships were measured using transthoracic echocardiographic and catheter-based PV loop analyses, respectively. While echocardiographic imaging is widely used as a non-invasive technique to assess cardiac physiology and architecture in rodent models of heart disease, PV-loops analysis is considered as the gold standard for hemodynamic assessment of ventricular performance (Lindsey, Kassiri et al. 2018). One of the main advantages of pressure-volume hemodynamic measurement over echocardiography is that PV-loops analyses are considered to relatively load-independent (Lindsey, Kassiri et al. 2018). Furthermore, the maximum pressure gradient that can be measure using pulsed-wave Doppler is about 60 mmHg (Lindsey, Kassiri et al. 2018). In terms of tissue Doppler imaging, the limitation is that it can only measure velocities parallel to the beam; hence, analyses of radial function are limited to the anterior and posterior walls, while the circumferential function is limited to the septal and lateral walls (Lindsey, Kassiri et al. 2018). Despite these limitations, echocardiography provides a non-

invasive cardiac functional analysis that simultaneously can be used to assess LV and left atrium (LA) structure and function. Also, echocardiography can be used for sequential analysis, where PV loops is terminal. Therefore, we used both state-of-the-art cardiac phenotyping techniques: transthoracic echocardiography and PV loop analysis. Cardioprotective roles of Ang-(1-7) have previously been studied in various preclinical investigations. Loot et al. showed for the first time that Ang-(1-7) treatment after myocardial infarction (MI), improved LV systolic pressure (LVP) and LV end-diastolic pressure (LVEDP) (Loot, Roks et al. 2002). Since then, different research groups have investigated the effects of Ang-(1-7) on the systolic and diastolic function of the heart. In a study using a transgenic murine model of diabetic cardiomyopathy and LV PV loop analysis, Mori et al. showed that Ang-(1-7) treatment improved EDPVR, Tau value, and IVRT, indicative of the effects of Ang-(1-7) on the improvement of active as well as passive relaxation phases of diastole (Mori, Patel et al. 2014). In our study, echocardiographic analyses identified modest improvements in IVRT as well as E/E', indices of LV diastolic function, within 4-weeks of Ang-(1-7) treatment. Furthermore, Ang-(1-7) treatment attenuated levels of LVEDP, which were increased in the HFD+L-NAME group. LVEDP, also commonly known as LV filling pressure, is considered an early indicator of ventricular remodeling and diastolic dysfunction. Tau value, a rate constant of exponential decay of the ventricular pressure, is widely used as a sensitive indicator of active relaxation properties of cardiac muscles. As the Tau value is calculated from the isovolumetric relaxation of the LV when the aortic and mitral valves are closed, it provides a preload-independent measurement of active isovolumetric relaxation of LV. 15-weeks of HFD+L-NAME resulted in increased Tau value indicative of a decreased rate of LV isovolumetric relaxation; 4-weeks Ang-(1-7) treatment reversed the Tau value which signified its potent effects on the active relaxation properties of the LV. As the changes in Tau value are

preload-independent, Ang-(1-7) effects on reversal of diastolic dysfunction can be correlated with its direct effects on left ventricular tissue, particularly cardiomyocytes. EDPVR relates to the passive filling curve of the left ventricle during diastole and is a measure of passive chamber stiffness (Burkhoff, Mirsky et al. 2005). Changes in EDPVR are reflective of the changes in myocardial material properties, chamber structural properties, and extracellular matrix organization (Burkhoff, Mirsky et al. 2005). An increase in EDPVR is indicative of an increase in myocardial stiffness or a decrease in compliance (Lindsey, Kassiri et al. 2018). In this study, the combination of HFD and L-NAME did not change the EDPVR, but the slightly increased in EDPVR after 15 weeks of HFD+L-NAME was moderately reduced with Ang-(1-7) treatment. Considering the reliance of the active relaxation phase on cellular metabolic activities and alteration in passive feeling being largely affected by ventricular wall stiffness, we hypothesized that diastolic dysfunction in the HFD+L-NAME group may be primarily mediated via metabolic perturbations. Importantly, metabolic dysfunction has previously been identified to play a key role in cardiac hypertrophy and ventricular concentric remodeling (Nakamura and Sadoshima 2018). As the EDPVR was largely unaffected in our study groups, we also hypothesized that the ventricular stiffness, particularly due to cardiac fibrosis, does not play a key role in HFD+L-NAME-mediated diastolic dysfunction. To study this hypothesis, the percentage of interstitial fibrosis was measured using PSR staining and confocal imaging analyses. Myocardial interstitial fibrosis (MIF) is classified as the diffuse, disproportionate accumulation of collagen in the myocardial interstitum (González, Schelbert et al. 2018). Using the PSR staining, MIF was characterized by the increase in the percentage of total myocardial tissue occupied by collagen fibers. Results from PSR staining were in line with PV loops data, showing a modest, albeit non-significant, increase in myocardial fibrosis after 15 weeks of HFD+L-NAME and was non-

significantly decreased with Ang-(1-7) treatment. Among different staining available for detecting the fibrosis level in the heart, PSR was indicated to provide the best contrast to differentiate collagen from cells (Schipke, Brandenberger et al. 2017). To confirm the findings from PSR staining, Masson Trichrome staining was also used to detect fibrosis level which showed similar results as shown by PSR staining.

Cardiac hypertrophy is characterized by an increase in cardiac mass and individual cardiomyocyte growth in both length and width (Nakamura and Sadoshima 2018). Uniform structural remodeling of the LV in cardiac hypertrophy can be measured using M-mode echocardiography (Lindsey, Kassiri et al. 2018). M-mode images provide a high temporal resolution of LV wall motion during systole and diastole from which contractile patterns and chamber size can be obtained (Lindsey, Kassiri et al. 2018). Using M-mode images of transthoracic echocardiography, reduced LV chamber size along with increased LV posterior wall thickness were observed, indicative of concentric remodeling and cardiac hypertrophy, in the HFD+L-NAME group. To validate the development of LV hypertrophy and study the cardiomyocyte size, WGA staining was used. Due to its affinity to N-acetyl glucosamine, WGA and myocyte cross-sectional area were measured. Although the existence of hypertrophy was confirmed with these experiments, Ang-(1-7) treatment did not show any significant effect on cardiomyocyte hypertrophy. Therefore, to understand whether Ang-(1-7) has a role in one of the key pathways related to hypertrophy, and also to confirm the development of hypertrophy and diastolic dysfunction was mostly due to metabolic dysfunction rather than increase level of fibrosis, different molecular pathways including alteration in the expression level of pAKT, pmTOR, pERK 1/2, pp38, pAMPK, pGSK3β, pJAK2, pSTAT3, and pPDH were evaluated. Sampaio et al., reported in 2007 that the Ang-(1-7)-MasR axis acted through the PI3K-AKT

pathway, to increase the phosphorylation of eNOS (Sampaio, Souza dos Santos et al. 2007). Activation of AKT by phosphorylation of Ser473 is known to antagonize different molecular pathways which have an essential role in the development of cardiac hypertrophy. Although no alteration was observed in the expression level of pAKT (ser473) after 15 weeks of HFD+L-NAME, 4-weeks treatment with Ang-(1-7) non-significantly increased the phosphorylation level of AKT by 23.28%, which is in line with previous studies indicative of ACE2/Ang-(1-7)/MasR axis actions being mediated via PI3K-AKT-eNOS pathways. Different *in vivo* and *in vitro* studies indicated the involvement of diverse protein pathways during the different phases of LV hypertrophy. Thus, we hypnotized that Ang-(1-7) can regress cardiac hypertrophy from molecular pathways that interact with PI3K-AKT-eNOS. mTOR, a major downstream component in the PI3K pathway, has been shown as a key regulator of cell and organ size by controlling the translational machinery in different *in vitro* and *in vivo* studies (Boluyt, Zheng et al. 1997, McMullen, Sherwood et al. 2004, Gao, Wong et al. 2006). Analysis of the expression level of mTOR phosphorylated at serine 2448 residue, indicated no significant changes in any of the study groups, which can indicate that cardiac hypertrophy in our experimental model may not be in the phase where mTOR activity is involved.

MAPK pathway is a signaling pathway that consists of sequentially acting protein kinases that participate in the regulation of cell growth, proliferation, differentiation, survival, transformation, and apoptosis (Shaul and Seger 2007). Three main branches of the MAPK signaling pathway are known as ERK 1/2, p38 kinases, and c-Jun N-terminal kinases (JNKs) (Mutlak and Kehat 2015). Different studies showed that activation of MAPKs ERK1/2 or p38 leads to the development of cardiac hypertrophy (Streicher, Ren et al. 2010, Mutlak and Kehat 2015). Knowing the essential role of Ang-(1-7) in inhibiting the activation of MAPKs,

phosphorylations of ERK1/2 and p38 were studied using Western blot analyses. The phosphorylated ERK1/2 expression level was increased with 15 weeks HFD+L-NAME, however, this increase was not significant (P=0.27). Treatment with Ang-(1-7) resulted in a significant decrease in phosphorylated form of ERK1/2, indicating a key role of, direct or indirect, inhibition of ERK1/2 in Ang-(1-7)-attenuated cardiac hypertrophy. Activation of JNK and p38 kinases is primarily associated with pro-inflammatory and stress-induced signal transduction, while ERK1/2 activation has more influence on cell growth and proliferation (Mutlak and Kehat 2015). Besides its role as a regulator of cardiac hypertrophy, ERK1/2 has an essential role in mitochondrial fission as evident by phosphorylating dynamin-related protein 1 (Drp1) in Ser616 residue (Gan, Huang et al. 2014, Serasinghe, Wieder et al. 2015). Since our results from PV loop analysis and IPGTT are indicative of metabolic dysfunction, non-significant increased in expression level of ERK1/2 and development of hypertrophy can be explained as metabolic dysfunction which was reversed with Ang-(1-7) treatment. Inhibition of p38 MAPK by Ang-(1-7) has been shown to block the development of LV remodeling (Patel, Zhong et al. 2016). The p38 MAPK pathway is an important intracellular signal transduction pathway involved in the production of proinflammatory and profibrotic mediators (Stambe, Atkins et al. 2004). Different studies have shown that the activation of p38 MAPK is necessary for the formation of fibrosis and cardiac deletion of p38 MPAK leads to inhibition of hypertrophy and improves diastolic function (Molkentin, Bugg et al. 2017). Using Western blot analysis, we did not observe a significant increase in phosphorylation of p38 MAPK after 15 weeks of HFD+L-NAME. This observation validated our previous findings and a sub-hypothesis that the development of hypertrophy and diastolic dysfunction in this study is a result of cardiac metabolic dysfunction.

GSK-3 is a ubiquitous serine/threonine-protein kinase and an important regulator of cardiac hypertrophy (Antos, McKinsey et al. 2002, Hirotani, Zhai et al. 2007). The activity of GSK-3β is controlled by the phosphorylation status of serine-9 residue. Phosphorylation of this site blocks GSK-3β activity by creating an inhibitory pseudosubstrate for the enzyme (Antos, McKinsey et al. 2002). The inactivation of GSK-3β has been demonstrated in heart failure patients (Hirotani, Zhai et al. 2007). Consistent with previous studies, we observed a significant increase in the expression level of the phosphorylated form of GSK-3β, indicating that 15 weeks of HFD+L-NAME inactivated GSK-3β. Four-weeks treatment of Ang-(1-7) did not lead to improvement in GSK3β expression, however, treatment with Ang-(1-7) led to non-significant decrease in the expression level of phosphorylated GSK-3β. The modest changes of pGSK3β by Ang-(1-7) indicated that Ang-(1-7) can moderately reverse the development of cardiac hypertrophy potentially through GSK3β, though it may require chronic Ang-(1-7) administration. Furthermore, it has been reported that GSK-3β regulates a wide range of cellular functions, including metabolism, gene expression, and cytoskeletal integrity (Grimes and Jope 2001). Therefore, modest activation of GSK-3β by Ang-(1-7) may have potential impact on improving cardiac metabolism.

Hypertrophic stimuli such as mechanical stretch, pressure overload, IL-6-related cytokines, and Ang II can activate cardiac Janus kinases- signal transducer and activator of transcription proteins (JAK-STAT) signaling (Booz, Day et al. 2002). Each of the proteins in the JAK-STAT pathway can cause different effects depending on the stimulus involved in its activation (Zhong, Wen et al. 1994). JAK2 activity modulates cardiac contractility indicating the importance of JAK2 as a key signaling component in the transition from cardiac growth to dysfunction (Wang, Fuhrer et al. 1995). Activated JAK2 can lead to the activation of ERK, JNK,

and p38 MAPK, stimulating pressure overload-induced hypertrophy (Beckles, Mascareno et al. 2006). Therefore, in this study, the phosphorylation level of JAK2 at Tyrosine residues (Tyr 1007/1008) was observed. 15 weeks of HFD+L-NAME did not alter the expression level of pJAK2 which can explain why the expression level of ERK1/2 and p38 MAPK did not change with HFD+L-NAME: one of the key signaling pathways that regulate ERK 1/2 and p38 MAPK phosphorylation was not affected in our study group. It has been suggested that phosphorylation of JAK2 stimulates the activation and phosphorylation of STAT3 protein (Giani, Gironacci et al. 2008). Different studies revealed the involvement of STAT3 in hypertrophy through its transcriptional roles (Harhous, Booz et al. 2019). Inhibition of STAT3 has been shown to attenuate the development of fibrosis and therefore regress cardiac remodeling (Mir, Chatterjee et al. 2012). In this study, the phosphorylation level of STAT3 in Serine and Tyrosine residue (Ser727 and Tyr705) has been detected. The expression level of STAT3 for both residues had a slight increase with HFD+L-NAME and treatment with Ang-(1-7) reduced the level of phosphorylated STAT3. However, these changes were not significant. The lower level of changes in STAT3 can be because of the fact that JAK2 expression was not altered in this study and therefore, the phosphorylation status of STAT3 was also not affected. STAT3 is also known to regulate genes involved in metabolism and mitochondrial activity (Harhous, Booz et al. 2019). Therefore, Ang-(1-7) mediating the phosphorylation level of STAT3 in both Ser727 and Tyr705 residues can block the formation of fibrosis as well as improving metabolic function in the heart and thus, attenuate cardiac remodeling.

AMPK is known as a metabolic master switch that mediates different intracellular systems, including the cellular uptake of glucose, β-oxidation of fatty acids, and biogenesis of Glucose transporter type 4 (GLUT4) (Arad, Seidman et al. 2007, Ouchi, Parker et al. 2011, Patel,

Mori et al. 2016). Furthermore, AMPK plays a protective role in the process of cardiac fibrosis by inhibiting the activity of ERK1/2 (Chen, Li et al. 2018, Li, Liu et al. 2019). Reduced ROS level with AMPK-dependent pathway which attenuates cardiac fibrosis was also demonstrated in several studies (Ma, Fu et al. 2015, Li, Liu et al. 2019). AMPK may also play a role in altering cardiac myocyte morphology and proliferation (Arad, Seidman et al. 2007), making it a key protein that warranted examination. In this study, a combination of HFD and L-NAME led to an inhibition of phosphorylation of AMPK, which is required for its activity. Decreased pAMPK levels indicated that the metabolic dysfunction and development of cardiac hypertrophy may be a result of a decreased AMPK activity. Four weeks treatment did not improve the expression level of pAMPK. . A regulator of AMPK-mediated metabolic modulation is PDH, a multienzyme complex located in the mitochondrial matrix. PDH activity is regulated via post-translational modification, particularly phosphorylation: PDH is inactivate in PDH kinase (PDK)-mediated phosphorylated state; PDH is active in PDH phosphatase-mediated dephosphorylated state (Stanley, Recchia et al. 2005). Downregulation of PDH activity (phosphorylation of PDH) has been observed in cardiac hypertrophy, diet-induced diastolic dysfunction, and Ang II-treated hearts (Stanley, Recchia et al. 2005, Mori, Basu et al. 2012, Patel, Mori et al. 2016). Similarly, phosphorylation and inactivation of PDH has been observed after 15 weeks of HFD+L-NAME, indicative of metabolic dysfunction which led to the development of hypertrophy. The effects of Ang-(1-7) on the expression level of pPDH was very low, which can be due to a short term of the treatment. Overall, the western blot analysis indicated that the development of hypertrophy, fibrosis, and metabolic dysfunction in this study can be result of partial activation of ERK1/2 and inactivation of AMPK, GSK3β, and PDH. Although Ang-(1-7) reversed the changes in

phosphorylation level of ERK1/2, it did not have a significant effect on the expression level of pAMPK, pGSK3β, and pPDH.

4.2. Conclusion

In this study, we found that 4-weeks treatment with Ang-(1-7) can attenuate the diastolic dysfunction and development of hypertrophy in a diet-induced murine model of HFpEF. Based on our in-depth investigation of various molecular pathways, we concluded that one of the molecular pathways from which Ang-(1-7) can improve metabolic function, reduce level of fibrosis, and therefore, decrease the level of cardiac hypertrophy which led to improved diastolic function is ERK1/2. However, due to non-significant changes in ERK1/2 expression level after 15 weeks of HFD+L-NAME, further study is needed to better understand the effect of Ang-(1-7) on ERK1/2. Furthermore, inactivation of GSK3β, AMPK, and PDH can explain the diastolic dysfunction and development of cardiac hypertrophy after 15 weeks of HFD+L-NAME which, in line with the echocardiography analysis, did not improve with Ang-(1-7) treatment.

4.3. Limitation

One of the major limitations of our study is the lack of investigations on the effects of Ang-(1-7) on the diet-induced HF in female mice. Various clinical studies indicated that the prevalence of HFpEF at any given age is higher in females than in males and therefore, females are physiologically more susceptible to HFpEF than male (Dunlay, Roger et al. 2017). Furthermore, the Olmsted County, Minnesota study indicated that 64% of patients with HFpEF were females (Gerber, Weston et al. 2015). However, using the combination of HFD and L-NAME on female mice aged 10-12 weeks, we did not observe the development of diastolic dysfunction and cardiac hypertrophy, which was consistent with the research group that

originally developed the HFpEF murine model (Tong, Schiattarella et al. 2019). Since HFpEF is a disorder of older age, we hypothesized that HFD+L-NAME can have a diverse effect on female mice and beginning of the HFD+L-NAME post-menopausally in female mice (9-month-old) may develop phenotype of HFpEF (Diaz Brinton 2012). However, the scope of our study did not allow for further studies. Determination of cardioprotective roles of Ang-(1-7) in female HFpEF murine model remains a critically important research question, which will require further detailed investigations.

4.4. Future direction

Considering the critical role of metabolic dysfunction in development of cardiac hypertrophy and diastolic dysfunction in the diet-induced murine model of HFpEF, effects of Ang-(1-7) on cardiac metabolic abnormalities using *ex vivo* working heart perfusion and *in vitro* studies on isolated adult cardiomyocytes are highly warranted. Using isolated working heart perfusion, parameters such as glycolysis, glucose oxidation, palmitate oxidation, and fatty acid oxidation (Belke, Larsen et al. 1999) can be investigated, which will shed the lights on intricacies of fuel consumption and energy production on the development of HFpEF and also on the effects of Ang-(1-7). The advantage of using an *ex vivo* working heart is that it has a very high level of sensitivity and the ability to control determinants of cardiac function such as afterload and perfusate. Furthermore, using extracellular flux (XF) analysis, mitochondrial bioenergetics in isolated mouse adult cardiomyocytes can be measure, which will help to determine the acute effects of Ang-(1-7) on cardiomyocytes' metabolic function. Using XF analysis, parameters such as extracellular acidification rate (ECAR), as a surrogate of glycolytic flux, and oxygen consumption rate (OCR), which represents mitochondrial respiration, (Readnower, Brainard et al. 2012) can be evaluated.

Knowing that the comorbidities such as pulmonary edema and renal dysfunction play a critical role in the mortality rate of patients with HFpEF, the long-term effects of HFD+L-NAME on the development the pathophysiology of HFpEF will provide the ability to investigate the effects of Ang-(1-7) on these comorbidities. Furthermore, since many of molecular pathways were not affected with Ang-(1-7) treatment, long-term experiments investigating the effects of Ang-(1-7) in the diet-induce murine HFpEF model will also help determine the chronic effects of Ang-(1-7) on structure and function of the heart, as well as different comorbidities associated with HFpEF.

Reference

Adamopoulos, S., et al. (2001). "A glossary of circulating cytokines in chronic heart failure." European journal of heart failure **3**(5): 517-526.

Antos, C. L., et al. (2002). "Activated glycogen synthase-3β suppresses cardiac hypertrophy in vivo." Proceedings of the National Academy of Sciences **99**(2): 907-912.

Bedi Jr, K. C., et al. (2016). "Evidence for intramyocardial disruption of lipid metabolism and increased myocardial ketone utilization in advanced human heart failure." Circulation **133**(8): 706-716.

Bertero, E. and C. Maack (2018). "Metabolic remodelling in heart failure." Nature Reviews Cardiology **15**(8): 457-470.

Boluyt, M. O., et al. (1997). "Rapamycin inhibits α1-adrenergic receptor–stimulated cardiac myocyte hypertrophy but not activation of hypertrophy-associated genes: evidence for involvement of p70 S6 kinase." Circulation research **81**(2): 176-186.

Borlaug, B. A. and M. M. Redfield (2011). "Diastolic and systolic heart failure are distinct phenotypes within the heart failure spectrum." Circulation **123**(18): 2006-2014.

Brutsaert, D. L. (2003). "Cardiac endothelial-myocardial signaling: its role in cardiac growth, contractile performance, and rhythmicity." Physiological reviews **83**(1): 59-115.

Bueno, O. F., et al. (2000). "The MEK1–ERK1/2 signaling pathway promotes compensated cardiac hypertrophy in transgenic mice." The EMBO journal **19**(23): 6341-6350.

Calvert, J. W., et al. (2011). "Exercise protects against myocardial ischemia–reperfusion injury via stimulation of β3-adrenergic receptors and increased nitric oxide signaling: role of nitrite and nitrosothiols." Circulation research **108**(12): 1448-1458.

Chioncel, O., et al. (2017). "Epidemiology and one-year outcomes in patients with chronic heart failure and preserved, mid-range and reduced ejection fraction: an analysis of the ESC Heart Failure Long-Term Registry." European journal of heart failure **19**(12): 1574-1585.

Cleland, J. G., et al. (2006). "The perindopril in elderly people with chronic heart failure (PEP-CHF) study." European heart journal **27**(19): 2338-2345.

De Boer, R. A., et al. (2003). "The imbalance between oxygen demand and supply as a potential mechanism in the pathophysiology of heart failure: the role of microvascular growth and abnormalities." Microcirculation **10**(2): 113-126.

Doenst, T., et al. (2013). "Cardiac metabolism in heart failure: implications beyond ATP production." Circulation research **113**(6): 709-724.

Dunlay, S. M., et al. (2017). "Epidemiology of heart failure with preserved ejection fraction." Nature Reviews Cardiology **14**(10): 591-602.

Edelmann, F., et al. (2013). "Effect of spironolactone on diastolic function and exercise capacity in patients with heart failure with preserved ejection fraction: the Aldo-DHF randomized controlled trial." Jama **309**(8): 781-791.

Flather, M. D., et al. (2005). "Randomized trial to determine the effect of nebivolol on mortality and cardiovascular hospital admission in elderly patients with heart failure (SENIORS)." European heart journal **26**(3): 215-225.

Fukushima, A. and G. D. Lopaschuk (2016). "Cardiac fatty acid oxidation in heart failure associated with obesity and diabetes." Biochimica et Biophysica Acta (BBA)-Molecular and Cell Biology of Lipids **1861**(10): 1525-1534.

Gan, X., et al. (2014). "Inhibition of ERK-DLP1 signaling and mitochondrial division alleviates mitochondrial dysfunction in Alzheimer's disease cybrid cell." Biochimica et Biophysica Acta (BBA)-Molecular Basis of Disease **1842**(2): 220-231.

Gao, X.-M., et al. (2006). "Inhibition of mTOR reduces chronic pressure-overload cardiac hypertrophy and fibrosis." Journal of hypertension **24**(8): 1663-1670.

Gembardt, F., et al. (2005). "Organ-specific distribution of ACE2 mRNA and correlating peptidase activity in rodents." Peptides **26**(7): 1270-1277.

Glezeva, N. and J. Baugh (2014). "Role of inflammation in the pathogenesis of heart failure with preserved ejection fraction and its potential as a therapeutic target." Heart failure reviews **19**(5): 681-694.

Goldberg, I. J., et al. (2012). "Lipid metabolism and toxicity in the heart." Cell metabolism **15**(6): 805-812.

Griendling, K. K., et al. (2000). "NAD (P) H oxidase: role in cardiovascular biology and disease." Circulation research **86**(5): 494-501.

Grimes, C. A. and R. S. Jope (2001). "The multifaceted roles of glycogen synthase kinase 3β in cellular signaling." Progress in neurobiology **65**(4): 391-426.

Halapas, A., et al. (2008). "In vivo models for heart failure research." in vivo **22**(6): 767-780.

Haq, S., et al. (2000). "Glycogen synthase kinase-3β is a negative regulator of cardiomyocyte hypertrophy." The Journal of cell biology **151**(1): 117-130.

Hilfiker-Kleiner, D., et al. (2006). "Molecular mechanisms in heart failure: focus on cardiac hypertrophy, inflammation, angiogenesis, and apoptosis." Journal of the American College of Cardiology **48**(9S): A56-A66.

Hirotani, S., et al. (2007). "Inhibition of glycogen synthase kinase 3β during heart failure is protective." Circulation research **101**(11): 1164-1174.

Ho, J. E., et al. (2012). "Discriminating clinical features of heart failure with preserved vs. reduced ejection fraction in the community." European heart journal **33**(14): 1734-1741.

Hung, M., et al. (2002). "Effect of verapamil in elderly patients with left ventricular diastolic dysfunction as a cause of congestive heart failure." International journal of clinical practice **56**(1): 57-62.

Inserte, J. and D. Garcia-Dorado (2015). "The cGMP/PKG pathway as a common mediator of cardioprotection: translatability and mechanism." British Journal of Pharmacology **172**(8): 1996-2009.

Kalogeropoulos, A., et al. (2010). "Inflammatory markers and incident heart failure risk in older adults: the Health ABC (Health, Aging, and Body Composition) study." Journal of the American College of Cardiology **55**(19): 2129-2137.

Kanwar, M., et al. (2016). "Targeting heart failure with preserved ejection fraction: current status and future prospects." Vascular health and risk management **12**: 129.

Keidar, S., et al. (2007). "ACE2 of the heart: from angiotensin I to angiotensin (1–7)." Cardiovascular research **73**(3): 463-469.

Konduracka, E., et al. (2007). "Diabetes-specific cardiomyopathy in type 1 diabetes mellitus: no evidence for its occurrence in the era of intensive insulin therapy." European heart journal **28**(20): 2465-2471.

Krüger, M., et al. (2009). "Protein kinase G modulates human myocardial passive stiffness by phosphorylation of the titin springs." Circulation research **104**(1): 87-94.

Liew, C. W., et al. (2017). "Multiphasic regulation of systemic and peripheral organ metabolic responses to cardiac hypertrophy." Circulation: Heart Failure **10**(4): e003864.

Loot, A. E., et al. (2002). "Angiotensin-(1–7) attenuates the development of heart failure after myocardial infarction in rats." Circulation **105**(13): 1548-1550.

Mann, D. L. (2002). "Inflammatory mediators and the failing heart: past, present, and the foreseeable future." Circulation research **91**(11): 988-998.

Massie, B. M., et al. (2008). "Irbesartan in patients with heart failure and preserved ejection fraction." New England Journal of Medicine **359**(23): 2456-2467.

McMullen, J. R., et al. (2004). "Inhibition of mTOR signaling with rapamycin regresses established cardiac hypertrophy induced by pressure overload." Circulation **109**(24): 3050-3055.

McMullen, J. R., et al. (2003). "Phosphoinositide 3-kinase (p110α) plays a critical role for the induction of physiological, but not pathological, cardiac hypertrophy." Proceedings of the National Academy of Sciences **100**(21): 12355-12360.

Mercure, C., et al. (2008). "Angiotensin (1-7) blunts hypertensive cardiac remodeling by a direct effect on the heart." Circulation research **103**(11): 1319-1326.

Mishra, S. and D. A. Kass (2021). "Cellular and molecular pathobiology of heart failure with preserved ejection fraction." Nature Reviews Cardiology: 1-24.

Mitschke, M. M., et al. (2013). "Increased cGMP promotes healthy expansion and browning of white adipose tissue." The FASEB Journal **27**(4): 1621-1630.

Molkentin, J. D., et al. (2017). "Fibroblast-specific genetic manipulation of p38 mitogen-activated protein kinase in vivo reveals its central regulatory role in fibrosis." Circulation **136**(6): 549-561.

Mori, J., et al. (2014). "Angiotensin 1–7 ameliorates diabetic cardiomyopathy and diastolic dysfunction in db/db mice by reducing lipotoxicity and inflammation." Circulation: Heart Failure **7**(2): 327-339.

Morimoto, H., et al. (2018). "Angiotensin 1–7 stimulates brown adipose tissue and reduces diet-induced obesity." American Journal of Physiology-Endocrinology and Metabolism **314**(2): E131-E138.

Mutlak, M. and I. Kehat (2015). "Extracellular signal-regulated kinases 1/2 as regulators of cardiac hypertrophy." Frontiers in pharmacology **6**: 149.

Nakamura, M. and J. Sadoshima (2018). "Mechanisms of physiological and pathological cardiac hypertrophy." Nature Reviews Cardiology **15**(7): 387-407.

Owan, T. E., et al. (2006). "Trends in prevalence and outcome of heart failure with preserved ejection fraction." New England Journal of Medicine **355**(3): 251-259.

Pacher, P., et al. (2008). "Measurement of cardiac function using pressure–volume conductance catheter technique in mice and rats." Nature protocols **3**(9): 1422.

Papinska, A. M., et al. (2016). "Long-term administration of angiotensin (1□ 7) prevents heart and lung dysfunction in a mouse model of type 2 diabetes (db/db) by reducing oxidative stress, inflammation and pathological remodeling." Pharmacological research **107**: 372-380.

Parajuli, N., et al. (2014). "Targeting angiotensin-converting enzyme 2 as a new therapeutic target for cardiovascular diseases." Canadian Journal of Physiology and Pharmacology **92**(7): 558-565.

Patel, V. B., et al. (2016). "ACE2 deficiency worsens epicardial adipose tissue inflammation and cardiac dysfunction in response to diet-induced obesity." Diabetes **65**(1): 85-95.

Patel, V. B., et al. (2015). "Antagonism of angiotensin 1–7 prevents the therapeutic effects of recombinant human ACE2." Journal of molecular medicine **93**(9): 1003-1013.

Patel, V. B., et al. (2014). "Angiotensin-Converting Enzyme 2 Is a Critical Determinant of Angiotensin II–Induced Loss of Vascular Smooth Muscle Cells and Adverse Vascular Remodeling." Hypertension **64**(1): 157-164.

Patel, V. B., et al. (2016). "Role of the ACE2/angiotensin 1–7 axis of the renin–angiotensin system in heart failure." Circulation research **118**(8): 1313-1326.

Paulus, W. J. and C. Tschöpe (2013). "A novel paradigm for heart failure with preserved ejection fraction: comorbidities drive myocardial dysfunction and remodeling through coronary microvascular endothelial inflammation." Journal of the American College of Cardiology **62**(4): 263-271.

Pavo, N., et al. (2016). "Renin-angiotensin system fingerprints of heart failure with reduced ejection fraction." Journal of the American College of Cardiology **68**(25): 2912-2914.

Ponikowski, P., et al. (2016). "2016 ESC Guidelines for the diagnosis and treatment of acute and chronic heart failure: The Task Force for the diagnosis and treatment of acute and chronic heart failure of the European Society of Cardiology (ESC) Developed with the special contribution of the Heart Failure Association (HFA) of the ESC." European heart journal **37**(27): 2129-2200.

Reddy, Y. N., et al. (2018). "A simple, evidence-based approach to help guide diagnosis of heart failure with preserved ejection fraction." Circulation **138**(9): 861-870.

Redfield, M. M., et al. (2013). "Effect of phosphodiesterase-5 inhibition on exercise capacity and clinical status in heart failure with preserved ejection fraction: a randomized clinical trial." Jama **309**(12): 1268-1277.

Sack, M. N., et al. (1996). "Fatty acid oxidation enzyme gene expression is downregulated in the failing heart." Circulation **94**(11): 2837-2842.

Sampaio, W. O., et al. (2007). "Angiotensin-(1-7) through receptor Mas mediates endothelial nitric oxide synthase activation via Akt-dependent pathways." Hypertension **49**(1): 185-192.

Santos, R. A. S., et al. (2019). "The renin-angiotensin system: going beyond the classical paradigms." American Journal of Physiology-Heart and Circulatory Physiology.

Santos, S. H. S., et al. (2010). "Improved lipid and glucose metabolism in transgenic rats with increased circulating angiotensin-(1-7)." Arteriosclerosis, thrombosis, and vascular biology **30**(5): 953-961.

Saxton, R. A. and D. M. Sabatini (2017). "mTOR signaling in growth, metabolism, and disease." Cell **168**(6): 960-976.

Schiattarella, G. G., et al. (2019). "Nitrosative stress drives heart failure with preserved ejection fraction." Nature **568**(7752): 351-356.

Schulz, E., et al. (2008). "Nitric oxide, tetrahydrobiopterin, oxidative stress, and endothelial dysfunction in hypertension." Antioxidants & redox signaling **10**(6): 1115-1126.

Serasinghe, M. N., et al. (2015). "Mitochondrial division is requisite to RAS-induced transformation and targeted by oncogenic MAPK pathway inhibitors." Molecular cell **57**(3): 521-536.

Sharma, K. and D. A. Kass (2014). "Heart failure with preserved ejection fraction: mechanisms, clinical features, and therapies." Circulation research **115**(1): 79-96.

Shaul, Y. D. and R. Seger (2007). "The MEK/ERK cascade: from signaling specificity to diverse functions." Biochimica et Biophysica Acta (BBA)-Molecular Cell Research **1773**(8): 1213-1226.

Shenouda, S. M., et al. (2011). "Altered mitochondrial dynamics contributes to endothelial dysfunction in diabetes mellitus." Circulation **124**(4): 444-453.

Shioi, T., et al. (2003). "Rapamycin attenuates load-induced cardiac hypertrophy in mice." Circulation **107**(12): 1664-1670.

Stambe, C., et al. (2004). "The role of p38α mitogen-activated protein kinase activation in renal fibrosis." Journal of the American Society of Nephrology **15**(2): 370-379.

Streicher, J. M., et al. (2010). "Novelty and Significance." Circulation research **106**(8): 1434-1443.

Surks, H. K., et al. (1999). "Regulation of myosin phosphatase by a specific interaction with cGMP-dependent protein kinase Iα." Science **286**(5444): 1583-1587.

Takimoto, E., et al. (2005). "Chronic inhibition of cyclic GMP phosphodiesterase 5A prevents and reverses cardiac hypertrophy." Nature medicine **11**(2): 214-222.

Tallant, E. A., et al. (2005). "Angiotensin-(1–7) inhibits growth of cardiac myocytes through activation of the mas receptor." American Journal of Physiology-Heart and Circulatory Physiology **289**(4): H1560-H1566.

Taube, A., et al. (2012). "Inflammation and metabolic dysfunction: links to cardiovascular diseases." American Journal of Physiology-Heart and Circulatory Physiology **302**(11): H2148-H2165.

Tian, N., et al. (2007). "Interactions between oxidative stress and inflammation in salt-sensitive hypertension." American Journal of Physiology-Heart and Circulatory Physiology **293**(6): H3388-H3395.

Torre-Amione, G. (2005). "Immune activation in chronic heart failure." The American journal of cardiology **95**(11): 3-8.

Valero-Muñoz, M., et al. (2017). "Murine models of heart failure with preserved ejection fraction: a "fishing expedition"." JACC: Basic to Translational Science **2**(6): 770-789.

van Heerebeek, L., et al. (2012). "Low myocardial protein kinase G activity in heart failure with preserved ejection fraction." Circulation **126**(7): 830-839.

van Heerebeek, L., et al. (2008). "Response to Letter Regarding Article,"Diastolic Stiffness of the Failing Diabetic Heart: Importance of Fibrosis, Advanced Glycation End Products, and Myocyte Resting Tension"." Circulation **117**(23): e484-e484.

Vargas-Castillo, A., et al. (2020). "Angiotensin-(1-7) induces beige fat thermogenesis through the Mas receptor." Metabolism **103**: 154048.

Weeks, K. L., et al. (2012). "Phosphoinositide 3-kinase p110α is a master regulator of exercise-induced cardioprotection and PI3K gene therapy rescues cardiac dysfunction." Circulation: Heart Failure **5**(4): 523-534.

Wei, A. E., et al. (2014). "Use of pressure-volume conductance catheters in real-time cardiovascular experimentation." Heart, Lung and Circulation **23**(11): 1059-1069.

Westermann, D., et al. (2011). "Cardiac inflammation contributes to changes in the extracellular matrix in patients with heart failure and normal ejection fraction." Circulation: Heart Failure **4**(1): 44-52.

Zhabyeyev, P., et al. (2013). "Pressure-overload-induced heart failure induces a selective reduction in glucose oxidation at physiological afterload." Cardiovascular research **97**(4): 676-685.

Zile, M. R., et al. (2004). "Diastolic heart failure—abnormalities in active relaxation and passive stiffness of the left ventricle." New England Journal of Medicine **350**(19): 1953-1959.

Zile, M. R., et al. (2011). "Prevalence and significance of alterations in cardiac structure and function in patients with heart failure and a preserved ejection fraction." Circulation **124**(23): 2491-2501.